

RESEARCH ARTICLE

Dual regulation of planar polarization by secreted Wnts and Vangl2 in the developing mouse cochlea

Elvis Huarcaya Najarro¹, Jennifer Huang¹, Adrian Jacobo², Lee A. Quiruz¹, Nicolas Grillet¹ and Alan G. Cheng^{1,*}

ABSTRACT

Planar cell polarity (PCP) proteins localize asymmetrically to instruct cell polarity within the tissue plane, with defects leading to deformities of the limbs, neural tube and inner ear. Wnt proteins are evolutionarily conserved polarity cues, yet Wnt mutants display variable PCP defects; thus, how Wnts regulate PCP remains unresolved. Here, we have used the developing cochlea as a model system to show that secreted Wnts regulate PCP through polarizing a specific subset of PCP proteins. Conditional deletion of *Wntless* or porcupine, both of which are essential for secretion of Wnts, caused misrotated sensory cells and shortened cochlea – both hallmarks of PCP defects. *Wntless*-deficient cochleae lacked the polarized PCP components *Dishevelled 1/2* and *frizzled 3/6*, while other PCP proteins (*Vangl1/2*, *Celsr1* and *dishevelled 3*) remained localized. We identified seven Wnt paralogues, including the major PCP regulator *Wnt5a*, which was, surprisingly, dispensable for planar polarization in the cochlea. Finally, *Vangl2* haploinsufficiency markedly accentuated sensory cell polarization defects in *Wntless*-deficient cochlea. Together, our study indicates that secreted Wnts and *Vangl2* coordinate to ensure proper tissue polarization during development.

KEY WORDS: Hair cell, Cell polarity, Wnt, Non-canonical, Frizzled, Dishevelled

INTRODUCTION

Planar cell polarity (PCP) signaling directs cell orientation within a tissue plane, a process fundamentally important to tissue assembly in multicellular organisms (Vladar et al., 2009). PCP signaling is mediated by six ‘core’ components, the asymmetric localization of which in the cell is a conserved molecular hallmark of planar polarization in invertebrate and vertebrate epithelia (Simons and Mlodzik, 2008; Wang and Nathans, 2007). At first, evenly distributed within cells, PCP components become asymmetrically localized as planar polarization is established, assembling into mutually exclusive complexes in opposite poles (Adler, 2012; Goodrich and Strutt, 2011; Singh and Mlodzik, 2012). Among these components, *frizzled* (*Fz/Fzd3* and *Fz/Fzd6*), *dishevelled* (*Dsh/Dvl1*, *Dsh/Dvl12* and *Dsh/Dvl13*) and *diego* (*Dgo/Ankrd6*) form complexes accumulating on one pole, while *Van Gogh* (*Vang/Vangl1* and *Vang/Vangl2*) and *Prickle* (*Pk/Pk1* and *Pk/Pk2*) enrich

on the other. *Flamingo* (*Fmi/Celsr1*, *Fmi/Celsr2* and *Fmi/Celsr3*) is present on both poles of the cell. Defective PCP signaling represented by a lack of polarized PCP components leads to congenital heart and tracheal abnormalities, skeletal dysplasia, neural tube defects as well as cochlear deformities (Butler and Wallingford, 2017; White et al., 2018). Despite their crucial roles, our understanding of upstream signals orchestrating PCP signaling is rather limited.


Wnt proteins have been implicated as upstream polarity cues for PCP signaling. For example, limb morphogenesis in mice requires a gradient of *Wnt5a*, which has been reported to act as an instructive cue to establish PCP (Gao et al., 2018, 2011). On the other hand, *Wnt11* can directly instruct alignment of muscle fibers in chick embryos (Gros et al., 2009), implying a contextual dependence on the Wnt member involved (van Amerongen and Nusse, 2009). However, in the wing epithelium of *Drosophila*, protocadherins (*Fat* and *Dachsous*) have been proposed as a long-range cue directing PCP core proteins (Ma et al., 2003), raising the possibility of Wnt-independent PCP mechanisms.

In *Drosophila*, misexpression of *Wnt4* or *Wg*, both Wnt proteins, can reorient cell polarity, implying a role for them in establishing a PCP orientation axis (Wu et al., 2013). Intriguingly, loss-of-function of both *Wg* and *Wnt4* has been reported to produce polarization defects, whereas deficiency of other Wnt members led to relatively mild PCP defects, supporting the notion of redundancy by multiple Wnts (Wu et al., 2013). In a similar vein, *Wnt5a* and *Wnt5b* are both required for the polarization of node cells and localization of the PCP core protein *Prickle2* (Minegishi et al., 2017). Moreover, the combination of *Wnt5b* and *Wnt11* guides planar polarization of zebrafish cardiomyocytes (Merks et al., 2018). Convergent extension (CE), a PCP-mediated phenomenon whereby tissues elongate axially by simultaneously narrowing and extending, is co-regulated by *Wnt5* and *Wnt11* during zebrafish gastrulation (Kilian et al., 2003).

As a classic model system to study planar polarization, the cochlea harbors intricately organized hair cells (HCs) crucial for hearing. HCs interdigitated by non-sensory supporting cells form an epithelial checkerboard longitudinally spanning three turns of the spirally shaped organ (Groves and Fekete, 2012). HCs are radially patterned as three outer rows and one inner row, all decorated with V-shaped stereocilia bundles pointing laterally towards their respective kinocilia (Basch et al., 2016). A body of literature indicates that PCP core proteins tightly control the synchronized and uniform orientation of HCs (Curtin et al., 2003; Etheridge et al., 2008; Jones et al., 2014; Montcouquiol et al., 2006; Torban et al., 2008; Wang et al., 2006a,b). On the other hand, although *Wnt5a* is required for limb development (Gao et al., 2018, 2011), only one-third of *Wnt5a* mutant mice display CE anomalies and mildly misrotated HCs in the cochlea (Qian et al., 2007), implying Wnt redundancy and/or Wnt-independent mechanisms. In agreement

¹Department of Otolaryngology-Head and Neck Surgery, Stanford University School of Medicine, Stanford, CA 94305, USA. ²Laboratory of Sensory Neuroscience, The Rockefeller University, New York, NY 10065, USA.

*Author for correspondence (agcheng@stanford.edu)

 A.J., 0000-0001-9381-6292; L.A.Q., 0000-0002-4518-6780; N.G., 0000-0001-8007-9246; A.G.C., 0000-0002-4702-8401

Handling Editor: Patrick Tam
Received 22 April 2020; Accepted 24 August 2020

with this notion, *Wnt5a* mutant cochleae displayed relatively normal *Vangl2* localization (Qian et al., 2007). Thus, the relationship between Wnts and PCP signaling remains unresolved.

Here, to circumvent Wnt redundancy and uncover the role(s) of secreted Wnts in PCP, we genetically ablated porcupine (*Porcn*) or Wntless (*Wls*), which are both essential for Wnt secretion, in the embryonic cochlea. In Wnt-producing cells, the generation of active Wnt proteins first requires lipidation by the O-acyltransferase enzyme Porcn (Nile and Hannoush, 2016; van den Heuvel et al., 1993). Lipidated Wnts are transported intracellularly by the chaperone protein *Wls* (Bänziger et al., 2006; Bartscherer et al., 2006), prior to secretion into the extracellular space (Herr et al., 2012). Genetic ablation of *Wls* and *Porcn* has been validated as an approach to uncover the function of secreted Wnts during development in various contexts (Barrott et al., 2011; Biechele et al., 2013; Carpenter et al., 2010, 2015; Jiang et al., 2013; Snowball et al., 2015). In both *Wls* and *Porcn*-deficient mice, we found defects in cochlear extension and HC polarization. Cochleae deficient in secreted Wnts maintained the asymmetric localization of the PCP core components *Vangl1/2*, *Celsr1* and *Dvl3*, but lost that of *Fz3/6* and *Dvl1/2*, suggesting differential sensitivities to the loss of secreted Wnts. We identified seven candidate Wnt ligands for mediating PCP in the embryonic cochlea, and found that *Wnt5a*, previously shown to mediate PCP signaling, was dispensable for cochlear extension, and polarization of hair cells and PCP proteins. Finally, we uncovered that *Vangl2* haploinsufficiency significantly accentuated hair cell polarization defects in Wnt-deficient cochlea, indicating a genetic interaction. Overall, our study delineates a dual regulation of planar polarization by secreted Wnts and *Vangl2* in the embryonic cochlea.

RESULTS

Wls and *Porcn* are expressed in the embryonic mouse cochlea

In the developing mouse inner ear, the cochlear duct first appears as a ventral protuberance around embryonic day (E) 12.5, and then lengthens over the subsequent week as sensory hair cells (HCs) are specified and planar polarized (Fig. 1A) (Wang et al., 2005). We first performed quantitative PCR (qPCR) to measure expression of *Wls* and *Porcn*, which are both required for Wnt secretion (van den Heuvel et al., 1993). Relative to E14.5, *Wls* expression displayed a slight decrease, while *Porcn* was significantly downregulated as the cochlea matured between E14.5–18.5 (Fig. 1B). Next, we performed *in situ* hybridization and immunostaining, and found that *Wls* was expressed within the embryonic cochlear duct (Fig. 1C–E,H, Fig. S1A–D). At stages prior to HC specification (E12.5 and E14.5), *Wls* mRNA and protein were detected in the roof and floor of the cochlear duct, including the *Sox2*⁺ prosensory domain where HCs are later specified (Fig. 1C–D). At E16.5 and E18.5, when planar polarity of HCs is established, *Wls* expression remained detectable in the cochlear duct but notably less intense in developing HCs (Fig. 1E,H and Fig. S1A–D). Similarly, *Porcn* mRNA was detected in the cochlear duct at E14.5 and E16.5 (Fig. 1F–G and Fig. S1G). Overall, these observations indicate that *Wls* and *Porcn* are both expressed in the embryonic cochlear duct before and during HC specification and polarization.

Wls is required for cochlear extension but dispensable for hair cell specification

The expression of *Wls* and *Porcn* suggests the presence of an active Wnt secretory pathway in the embryonic cochlear duct. To assess the role of *Wls* in cochlear development, we generated *Emx2*^{Cre/+};

Wls^{fl/fl} (*Wls* cKO) to conditionally ablate *Wls* in the cochlear duct. *Emx2*-Cre driver has been previously used to study PCP in the cochlea and its Cre activity is specifically detected in the cochlear duct (Fig. S2A) (Ghimire and Deans, 2019; Kimura et al., 2005; Ono et al., 2014); this approach allowed us to circumvent embryonic lethality resulting from *Wls* germline deletion (Carpenter et al., 2010). Indeed, *Wls* cKO embryos were viable until birth, although they displayed gross limb and craniofacial morphological abnormalities (Fig. S2B–E). Using *Wls* antibody staining and *in situ* probes against *Wls*, we determined that *Wls* protein and mRNA were effectively ablated from the cochlear duct in E13.5 and E18.5 *Wls* cKO animals (Fig. 1I,K,L, Fig. S3A–F). As expected, *Wls* expression remained outside the cochlear duct in *Wls* cKO animals (Fig. 1I,K, Fig. S3B,E,F) and throughout the cochlea in control animals (*Emx2*^{Cre/+}; *Wls*^{+/fl}, Fig. 1H,J, Fig. S3A,C,D). These experiments confirm the specificity and efficiency of the *Emx2*-Cre mouse line to delete *Wls* from the cochlear duct before HC specification and the establishment of HC planar polarization.

Next, to begin to characterize the cochlea from *Wls* cKO animals, we measured the cochlear length. At E18.5, *Wls* cKO cochleae appeared wide and were significantly shorter in comparison with controls (2313.5±374.6 and 4683.0±279.0 μm, respectively, *P*<0.001) (Fig. 1K,M), suggesting that *Wls*-mediated Wnt secretion is required for cochlear extension.

To confirm a role for Wnt secretion, we also examined the *Porcn*-deficient cochleae. We first examined the *Emx2*^{Cre/+}; *Porcn*^{fl/y} animals and no cochlear shortening or planar polarization defects were detected (not shown). Because previous studies indicated that *Porcn* is a highly stable protein (Kadowaki et al., 1996; Rios-Estevés et al., 2014), we decided to use *Pax2*-Cre to ensure an early ablation of *Porcn*. We examined *Pax2*-Cre; *Porcn*^{fl/y} (*Porcn* cKO) mouse line, in which *Porcn* mRNA deletion was confirmed within the cochlear duct (Fig. S4A–F). We also performed qPCR and confirmed a significant decrease in *Porcn* mRNA in these mutant animals (Fig. S4M). *Pax2*-Cre; *Wls*^{fl/fl} mice failed to develop any cochlear structures (data not shown) and were therefore not examined further. Like the *Wls* cKO cochlea, *Porcn* cKO cochleae appeared wider and were also significantly shorter than controls (*Pax2*-Cre; *Porcn*^{y/fl}, Fig. S4N) (Liu et al., 2012; Ohyama and Groves, 2004).

To determine whether HCs were specified, we stained and detected Atoh1- and Myosin7a-expressing HCs in *Wls* cKO and *Porcn* cKO cochleae (Fig. 2A–D, Figs S4K,L and S5A–D), confirming that HC specification was preserved in cochlear duct deficient in secreted Wnts. However, unlike control cochlea, where HCs were arranged as four rows, both *Wls* and *Porcn* cKO cochleae were widened and displayed supernumerary rows of hair cells, a phenotype consistent with convergent extension defects (Fig. S6A,B,E–H) (Chacon-Heszele et al., 2012; May-Simera and Kelley, 2012; Montcouquiol et al., 2003; Wang et al., 2006a, 2005). We did not rule out a decrease in cell proliferation in the *Wls* cKO and *Porcn* cKO cochleae, which could have also contributed to the shorter cochlear phenotype, as proliferation of sensory progenitors is shown to depend on Wnt signaling *in vitro* (Jacques et al., 2012). Overall, these data indicate that Wnt secretion is required for cochlear extension but is dispensable for HC specification.

Wls deletion perturbs hair cell orientation

Perturbed PCP signaling is manifested as a shortened and widened cochlea harboring supernumerary rows of misoriented hair cells (May-Simera and Kelley, 2012). To further characterize PCP defects in *Wls* cKO and *Porcn* cKO animals, we analyzed stereocilia bundle orientation in HCs, which is a readout for the integrity of the

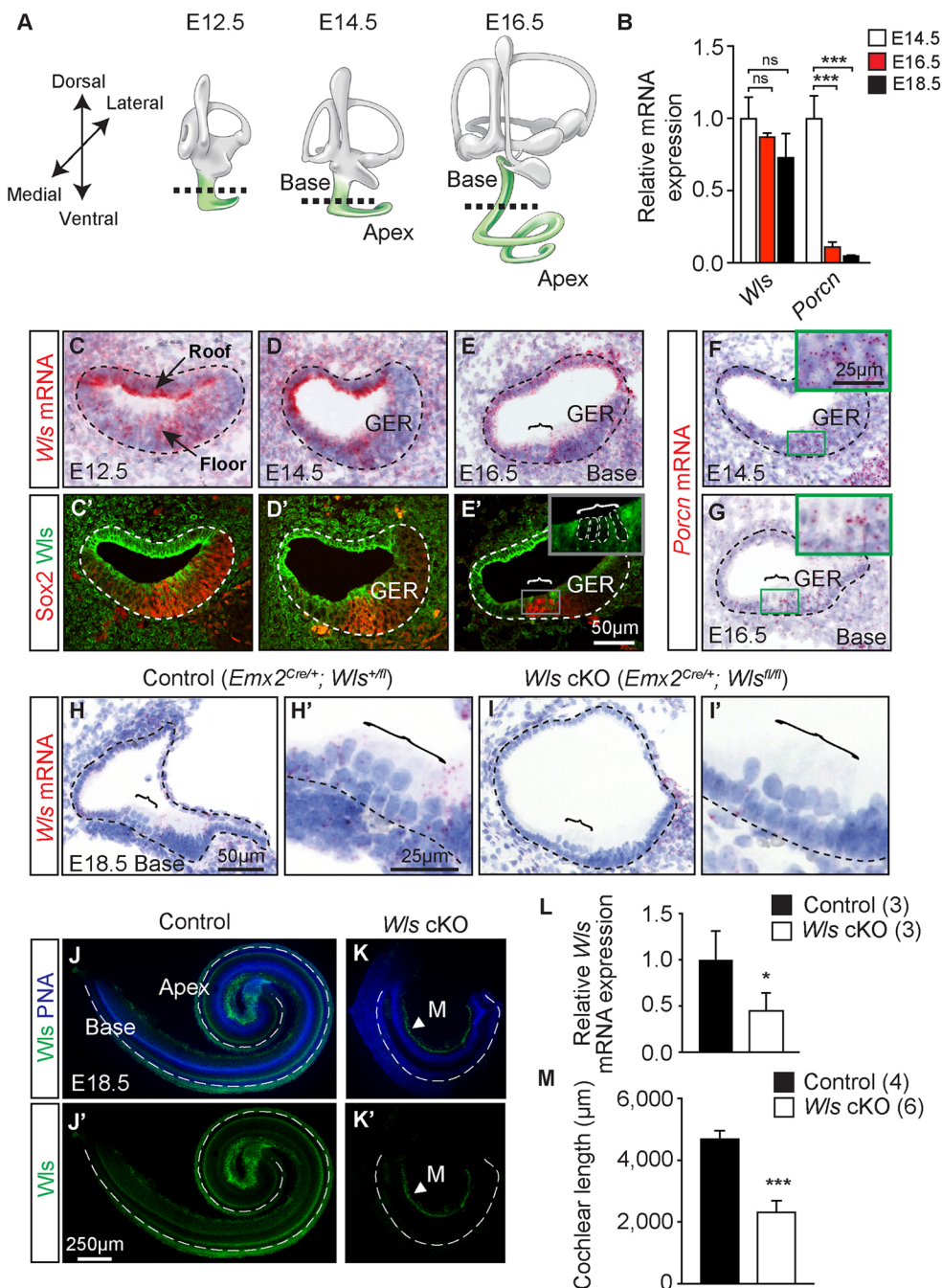


Fig. 1. Genetic ablation of *Wntless* in the embryonic cochlear duct. (A) Different stages of cochlear development. After E12.5, the cochlea develops as a ventral outpouching and subsequently lengthens to form the cochlear duct. Dashed line marks basal turns shown as sections in C-E. (B) qPCR shows persistent expression of *Wntless* (*Wls*) in the embryonic cochlea. In contrast, porcupine (*Porcn*) expression decreased after E14.5. $n=3$ for each age group. (C-G) RNAscope *in situ* hybridization demonstrating *Wls* and *Porcn* mRNA expression inside the cochlear duct, where *Wls* protein is also detected. Dashed line marks the cochlear duct. (E,E') At E16.5, *Wls* expression was high in *Sox2*⁺ supporting cells and low/absent in hair cells. (F,G) *Porcn* mRNA expression was detected inside the cochlear duct at E14.5 and E16.5. (H,I) *Wls* mRNA expression in cochlear duct of E18.5 *Emx2*^{Cre/+}; *Wls*^{+/fl} (control) mice and a drastic reduction in *Emx2*^{Cre/+}; *Wls*^{fl/fl} (*Wls* cKO). (H',I') Higher-magnification views of the organ of Corti. (J-K') *Wls* cKO cochlea displayed a marked reduction in *Wls* expression and length compared with control. PNA marks the cell membrane. *Wls* protein remained detectable in the modiolus (arrowhead) outside the cochlear duct. Dashed lines mark the lateral aspect of the organ of Corti. (L) Quantification showing significantly lower expression *Wls* mRNA in *Wls* cKO cochlea relative to controls. (M) *Wls* cKO cochleae are significantly shorter than control organs. Two-tailed Student's *t*-test, *** $P<0.001$, * $P<0.05$. Data are mean±s.d. M, modiolus; GER, greater epithelial ridge. Brackets indicate the organ of Corti.

PCP pathway (May-Simera, 2016). We examined the basal and middle turns of E18.5 cochleae, where HCs typically show a clear planar polarization by this age. In control cochlea, a uniform orientation of stereocilia bundles was observed along the mediolateral axis for both outer (OHCs) and inner hair cells (IHCs) (Fig. 2E,F, Fig. S6A). In the *Wls* cKO cochleae, we noted supernumerary rows of HCs with aberrantly oriented stereocilia bundles, with defects most severe among IHCs and the outermost rows of OHCs in both the basal and middle turns (Fig. 2G, Fig. S6B). When each row of HCs was individually measured, the orientation of stereocilia bundles of IHCs and OHCs had significantly greater deviation in *Wls* cKO than those in the control cochleae, indicating a PCP defect ($n=232$ *Wls* cKO IHCs and 616 OHCs, and 171 control IHCs and 575 OHCs, $P<0.01-0.001$, Fig. 2H and Fig. S6C,D). Since the *Wls* cKO cochleae were

significantly shorter than control cochleae, we also compared the base of *Wls* cKO cochleae with the middle turn of control cochlea. Consistent with the above results, we found significantly greater deviation in stereocilia bundle orientation in *Wls* cKO compared with control cochleae ($n=232$ *Wls* cKO IHCs and 616 OHCs, and 166 control IHCs and 511 OHCs, $P<0.05$). In parallel, we also detected defects in HC polarization in *Porcn* cKO cochlea (Fig. S6E-H). Together, these data indicate that Wnt secretion from the cochlear duct is required for proper HC polarization in the developing cochlea. In addition, the HC polarization defects observed in *Wls* and *Porcn* cKO are similar but milder compared with those in mutants lacking PCP core components (Curtin et al., 2003; Etheridge et al., 2008; Jones et al., 2014; Montcouquiol et al., 2006; Torban et al., 2008; Wang et al., 2006a,b). It is likely that redundant mechanisms regulate planar polarization of HCs in the

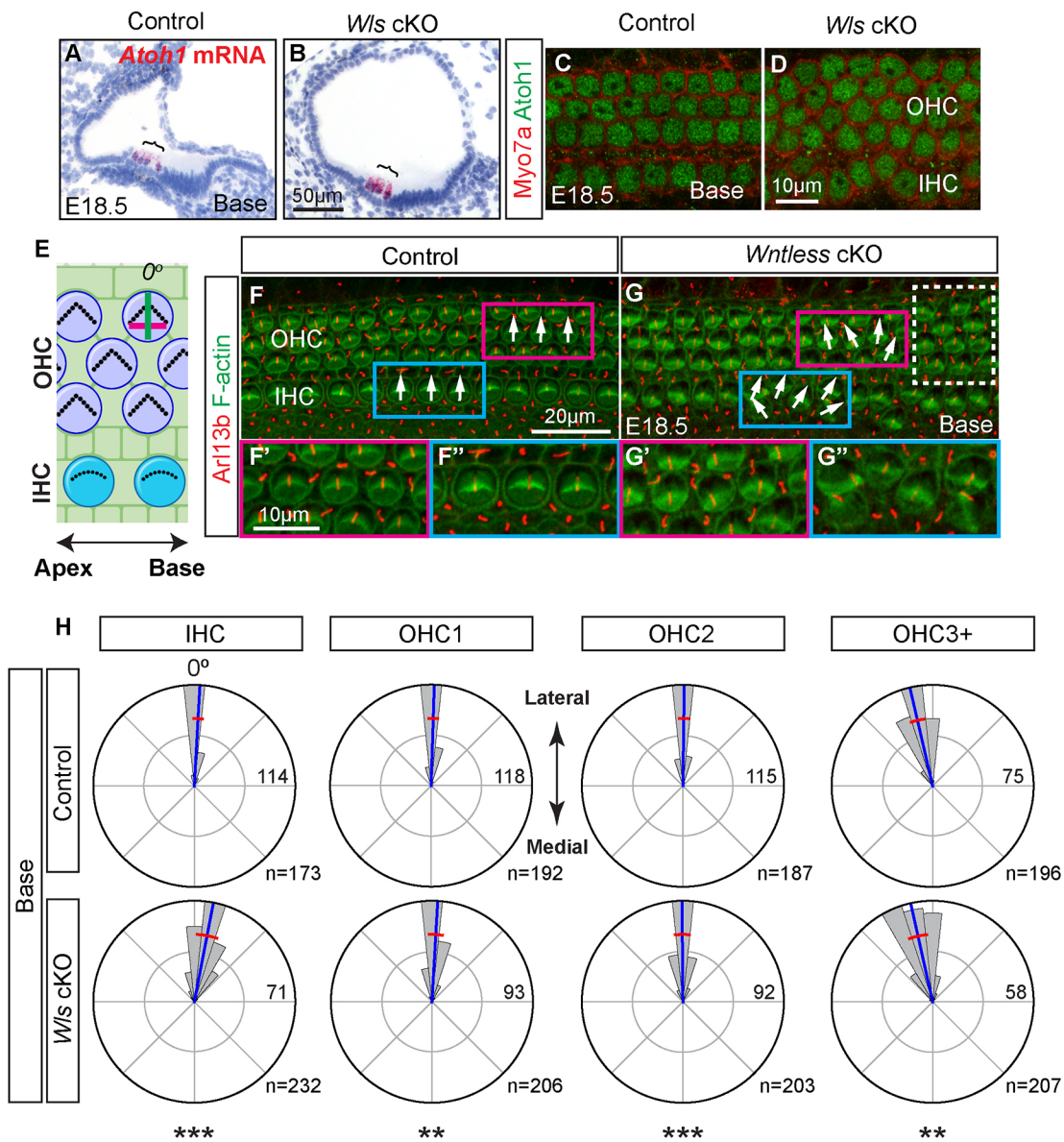


Fig. 2. *Wls* is dispensable for hair cell specification but is required for planar cell polarity. (A,B) Cochlear sections showing *Atoh1* mRNA expression in both control (*Emx2^{Cre/+}; Wls^{+/fl}*) and *Wls* cKO (*Emx2^{Cre/+}; Wls^{fl/fl}*) hair cells. Brackets indicate the organ of Corti. (C) Control cochlea displaying three rows of outer hair cells (OHCs) and one row of inner hair cells (IHCs). (D) In contrast, *Wls* cKO cochlea shows extranumerary and disorganized rows of HCs. Myosin7a and *Atoh1* expression was seen in both control and *Wls* cKO cochlea. (E) Schematic of the organ of Corti depicting stereocilia bundle orientation at zero degrees with respect to the mediolateral axis of the cochlea (green line). The line perpendicular to this axis is in purple. (F,G) Whole-mount cochlea stained for F-actin and Arl13b (kinocilia). Stereocilia bundles of OHCs (F') and IHCs (F'') in control cochlea were consistently oriented along the mediolateral axis (arrows). *Wls* cKO cochlea displayed aberrant stereocilia bundle orientation of OHCs (G') and IHCs (G'') (arrows). Both extranumerary OHCs (dashed box) and IHCs (G'') were noted in *Wls* cKO cochlea. White arrows indicate the orientation of stereocilia bundles. (H) Rose diagrams showing measurements of the angular orientation of OHCs and IHCs from control and *Wls* cKO cochleae (basal turn shown). Individual HCs were grouped and plotted into bins 15 degrees wide. The length of each petal represents the number of HCs therein, with the number of the longest petal (also the radius of the outer circle) indicated. The radius of the inner circle is half of the outer circle. Individual rows of HCs from *Wls* cKO cochleae displayed significantly more variation in stereocilia bundle orientations than those from control. The OHC3+ group included the third and other more-lateral rows of OHCs. Zero degrees represents the mediolateral axis. *n*, number of hair cells measured, collected from six control and *Wls* cKO cochleae. Circular mean and s.d. are indicated with blue and red lines, respectively. Permutation test of equality of variances used (see Materials and Methods section for more details). ***P*<0.01, ****P*<0.001.

cochlear duct. For example, it is possible that Wnts originating from the periotic mesenchyme outside the cochlear duct also play a role in governing hair cell polarity.

Mislocalization of PCP components in the absence of *Wls*

To determine the mechanisms underlying defects of cochlear extension and HC polarity in Wnt-deficient cochleae, we next assessed whether components of PCP signaling were perturbed.

One striking feature of planar polarization in the cochlea is the asymmetric localization of PCP core proteins in the organ of Corti, with Dvl2 and Dvl3 at the lateral pole and Fz3 and Fz6 at the medial pole of HCs. On the other hand, Vangl1 is detected in the lateral side of neighboring supporting cells, whereas Celsr1 is enriched at the junction between the medial side of HC and lateral side of neighboring supporting cells (Fig. 3A) (Duncan et al., 2017; Rida and Chen, 2009). In E18.5 control tissues, Fz6 and Dvl2 were

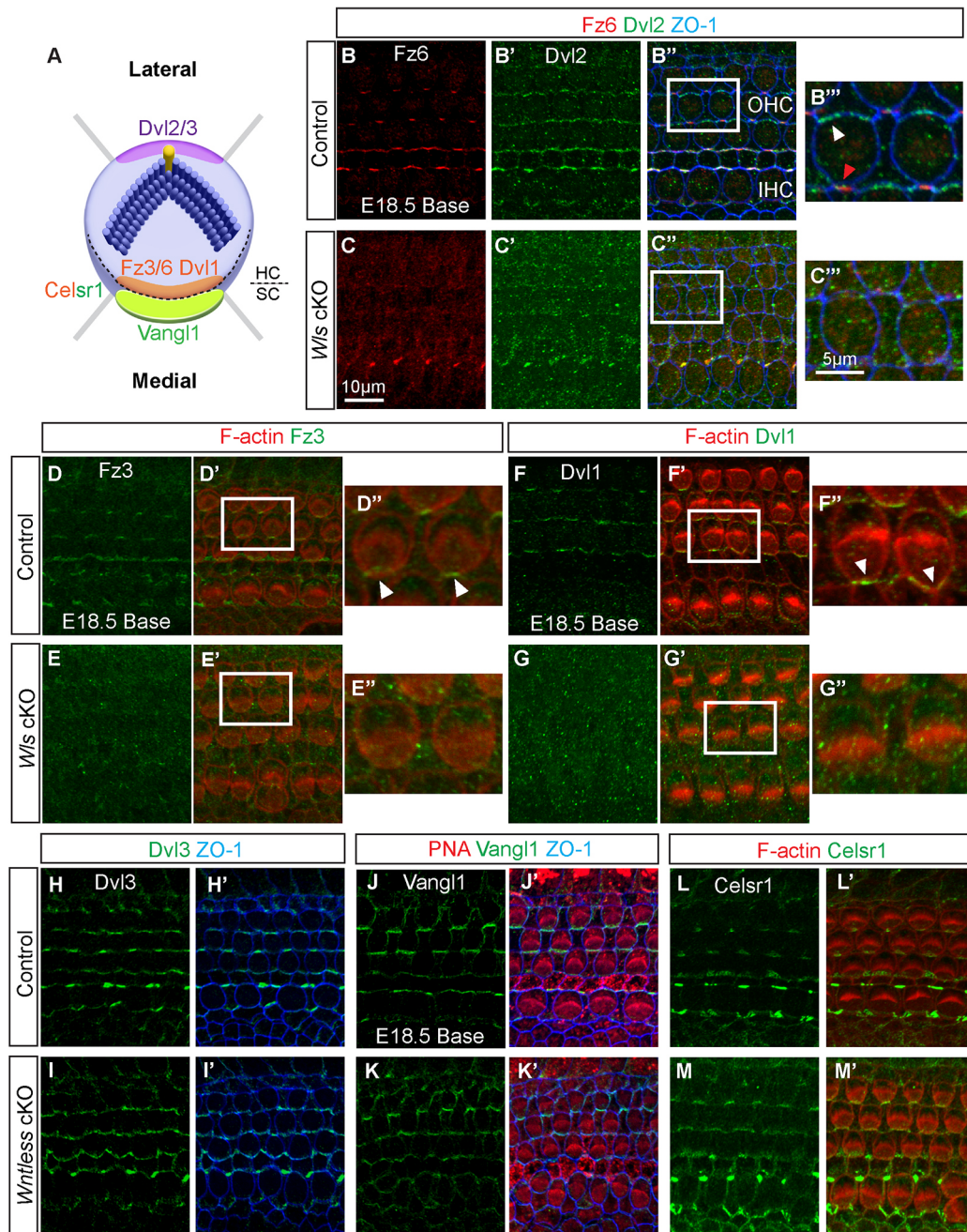


Fig. 3. *Ws* is required for polarization of planar cell polarity core components. (A) Cartoon depicting asymmetric localization of PCP core proteins in the organ of Corti. Dishevelled (Dvl) 2 and Dvl3 reside on the lateral pole of hair cells (HCs) and frizzled (Fz) 3 and Fz6 on the medial pole. Vangl1 is present at the lateral pole of supporting cells and Celsr1 is enriched at the junction between the medial side of HC and lateral side of neighboring SCs. (B-C'') In control cochlea (*Emx2^{Cre/+}; Ws^{+/fl}*), Fz6 (B) and Dvl2 (B') were asymmetrically localized in the medial and lateral aspects of HCs, respectively. ZO-1 marks tight junctions between HCs and supporting cells. In *Ws* cKO cochlea, no apparent asymmetric localization of Fz6 (C) and Dvl2 (C') was detected. (D-E'') Localized expression of Fz3 was detected in control cochlea, but not in the *Ws* cKO cochlea. (F-G'') In control cochleae, Dvl1 was localized to the medial poles of HCs (arrowheads). This asymmetric localization was not detected in *Ws* cKO HCs. (H-I'') Co-immunostaining of Dvl3 and ZO1 showing lateral localization of Dvl3 in HCs in control and *Ws* cKO cochleae. (J-K'') In control and *Ws* cKO cochleae, Vang1 expression was localized at the lateral pole of supporting cells. Peanut agglutinin (PNA) marks hair cell stereocilia bundles. (L-M'') Localized expression of Celsr1 expression was seen in both control and *Ws* cKO cochleae. For all images, the basal turn is shown. Cochleae from three control and *Ws* cKO animals were analyzed. Scale bars in C and C'' can be applied to all panels.

clearly polarized to the medial and lateral poles of HCs, respectively (Fig. 3B, Fig. S7B), consistent with previous reports (Wang et al., 2006a,b). By contrast, expression of Fz6 and Dvl2 was uniformly non-polarized in HCs of *Ws* cKO cochleae (Fig. 3C, Fig. S7C). Similarly, asymmetric localization of both Fz6 and Dvl2 was sharply diminished in HCs in *Porc* cKO cochleae (Fig. S8A,B).

We next examined Fz3 and Dvl1, which have been shown to serve redundant functions with Fz6 and Dvl2, respectively, in establishing PCP in the cochlea (Etheridge et al., 2008; Wang et al., 2006b). In control cochlea, Dvl1 and Fz3 were seen polarized to the medial pole of HCs and at the junction with adjacent supporting cells (Fig. 3D,F, Fig. S7D,F). Compared with control, Dvl1 and Fz3 were

non-localized in *Wls* cKO HCs (Fig. 3E,G, Fig. S7E,G). These data suggest that secreted Wnts influence proper asymmetric localization of Dvl1/2 and Fz3/6 proteins in HCs.

We next examined the localization of Dvl3, Vangl1 and Celsr1 proteins. Interestingly, Dvl3 protein remained polarized to the lateral pole of hair cells in both control and *Wls* cKO cochleae (Fig. 3H,I, Fig. S7H,I). Moreover, both Vangl1 and Celsr1 remained asymmetrically localized in *Wls* cKO cochleae akin to control tissues (Fig. 3J-M, Fig. S7J-M), although subtle changes in their localization or level of expression cannot be ruled out. In summary, these results indicate that asymmetric localization of a specific subset of core PCP proteins is dependent on secreted Wnts in the cochlear duct.

Abnormal kinocilia positioning in *Wls* cKO cochlea

In the cochlea, mutations in PCP pathway components can cause stereocilia bundle orientation defects that are coupled with kinocilium and basal body positioning defects (Montcouquiol et al., 2003). We next sought to examine the relationship between these HC organelles in *Wls* cKO cochleae. We first assessed kinocilia integrity by immunostaining for its components and its associated basal body (Fig. 4A). In control and *Wls* cKO HCs, we detected colocalization of Arl13b and acetylated tubulin (both kinocilium), as well as Rpgrip1L (transitional zone). Similarly, the basal body marker pericentrin was also present in both control and *Wls* cKO HCs (Fig. 4B,C,L-Q). In addition, we found a normal expression pattern of Arl13b and pericentrin in *Porcn* cKO cochleae (Fig. S6G,H).

Next, we analyzed the position of basal bodies and kinocilia. In control tissues, these organelles were found at the lateral pole adjacent to the vertex of stereocilia bundles (Fig. 4B). The position of the kinocilium was further confirmed by scanning electronic microscopy (SEM) (Fig. 4D,F,G). In *Wls* cKO cochlea, the kinocilia and corresponding basal bodies in both IHCs and OHCs were frequently off-centered and positioned away from the vertex of stereocilia bundles (Fig. 4C-E), both defects confirmed in OHCs and IHCs under SEM (Fig. 4E,H-K). We next stained control and *Wls* cKO tissues to further assay kinocilium positioning using Arl13b and Rpgrip1L antibodies (Fig. 4L,Q). These markers similarly showed that kinocilium position was localized to the lateral pole in control HCs, and also confirmed abnormal positioning of kinocilia in *Wls* cKO HCs (Fig. 4N-Q, Fig. S9B,D). Using pericentrin and Arl13b labeling, we also observed kinocilium positioning defects in *Porcn* cKO HCs (Fig. S6G,H). These experiments indicate that kinocilium and basal positioning are abnormal in HCs of *Wls* cKO and *Porcn* cKO cochleae.

To further characterize the kinocilium-positioning defects in *Wls* cKO, we plotted the position of kinocilium (based on Rpgrip1L expression) from individual HCs ($n=92$ *Wls* cKO IHCs and 306 OHCs, and 82 control IHCs and 261 OHCs). Qualitatively, kinocilium position in *Wls* cKO HCs was more variable than in controls (Fig. 4R, Fig. S9E,F). However, similar to controls, we found a highly positive correlation between the angles of kinocilium and stereocilia bundles in *Wls* cKO cochleae (base, $r=0.76$; middle, $r=0.83$; both $P<0.001$, Fig. 4S, Fig. S9G,H), suggesting that organization of the two processes remained coupled similar to mutants of the PCP pathway (Montcouquiol et al., 2003).

Aberrant kinocilium positioning has also been observed in cochlea with defective intrinsic cell polarity, although these defects are coupled with malformed stereocilia bundles (Tarchini et al., 2013), which was not apparent in either *Wls* cKO or *Porcn* cKO cochleae. We assayed the integrity of this pathway by

immunostaining for the intrinsic cell polarity markers LGN and $\text{G}\alpha\text{i}3$, which are expressed in the lateral apical surface of HCs, and $\text{Pard}6$, which is found on the medial apical surface (Fig. S10A) (Ezan et al., 2013; Tarchini et al., 2013). LGN, $\text{G}\alpha\text{i}3$ and $\text{Pard}6$ were all asymmetrically localized in both control and *Wls* cKO HCs (Fig. S10B-G), suggesting that asymmetric localization of these intrinsic cell polarity proteins is not dependent on *Wls*. However, our results do not rule out subtle defects in intrinsic cell polarity, as suggested by the findings of off-centered kinocilia. Overall, these data indicate intact, but mislocalized, kinocilia, in HCs of a cochlear duct deficient in secreted Wnts, with defects in positioning highly correlated with stereocilia bundle orientation defects.

Expression of Wnt ligand candidates in the embryonic cochlear duct

Thus far, our observations indicate that ablation of the Wnt secretory pathway in the cochlear epithelium perturbs PCP in the developing cochlea. We next sought to identify the Wnt ligands expressed in the cochlear duct. To this end, we first performed qPCR on whole cochleae and found 12 Wnt genes (*Wnt2*, *Wnt2b*, *Wnt3*, *Wnt4*, *Wnt5a*, *Wnt5b*, *Wnt6*, *Wnt7a*, *Wnt7b*, *Wnt9a*, *Wnt11* and *Wnt16*) consistently expressed between E14.5 and E18.5 (Fig. 5A, Fig. S11A). Next, via *in situ* hybridization, seven Wnts (*Wnt2b*, *Wnt4*, *Wnt5a*, *Wnt7a*, *Wnt7b*, *Wnt9a* and *Wnt11*) were specifically detected in the cochlear duct at E14.5 and E16.5 (Fig. 5B-H, Fig. S11B-H). We observed robust expression of *Wnt4*, *Wnt5a*, *Wnt7a* and *Wnt7b* in E14.5 and E16.5 cochlear duct (Fig. 5C-F, Fig. S11C-F). Expression of *Wnt2b*, *Wnt9a* and *Wnt11* was also detected in the cochlear duct, albeit at low levels (Fig. 5B,G,H, Fig. S11B,G,H). These results indicate that multiple Wnts are expressed in the embryonic cochlea, and seven of them are specifically expressed in the cochlear duct.

As *Wnt5a* is highly expressed in the cochlear duct and has been implicated in PCP in multiple contexts, including the embryonic cochlea (Wang et al., 2005), we asked whether *Wnt5a* mediates the PCP defects in Wnt-deficient cochlea. To test this hypothesis, we used a validated *Wnt5a* floxed allele (Ryu et al., 2013) to generate *Emx2^{Cre/+}; Wnt5a^{fl/fl}* mice (*Wnt5a* cKO) and examined its effects on HC orientation at E18.5. Despite loss of *Wnt5a* mRNA signals in the cochlear duct (Fig. 5J,K), we unexpectedly detected no cochlear extension defects in *Wnt5a* cKO animals (Fig. S12A-C). As in controls, HCs displayed polarized expression of Fz6 and Vangl2 (Fig. 5L-O) and showed no defects in stereocilia bundle orientation (Fig. 5P,Q, Fig. S12D,E). Together, these results demonstrate candidate Wnt ligands that regulate PCP in the cochlea. Ablation of *Wnt5a* in the cochlear duct does not cause morphological or molecular PCP defects in the embryonic cochlea, suggesting that PCP is not dependent on *Wnt5a* alone or that other Wnts compensate for the *Wnt5a* loss.

Wls genetically interact with *Vangl2* to orient hair cells in the embryonic cochlea

We next examined *Wls* cKO for asymmetric localization of Vangl2, which is required for HC orientation (Montcouquiol et al., 2006). In both control and *Wls* cKO cochleae, the polarized expression of Vangl2 was observed in the lateral side of supporting cells (Fig. 6A-C, Fig. S13A-C), suggesting that conditional ablation of *Wls* from the cochlear duct is not sufficient to affect the asymmetric localization of Vangl2. Alternatively, it is possible that Vangl2 localization does not depend on secreted Wnts in the cochlear duct.

Because ablation of *Wls* led to a loss of asymmetry of Fz3, Fz6, Dvl1 and Dvl2 in and mild PCP defects of HCs, we asked whether

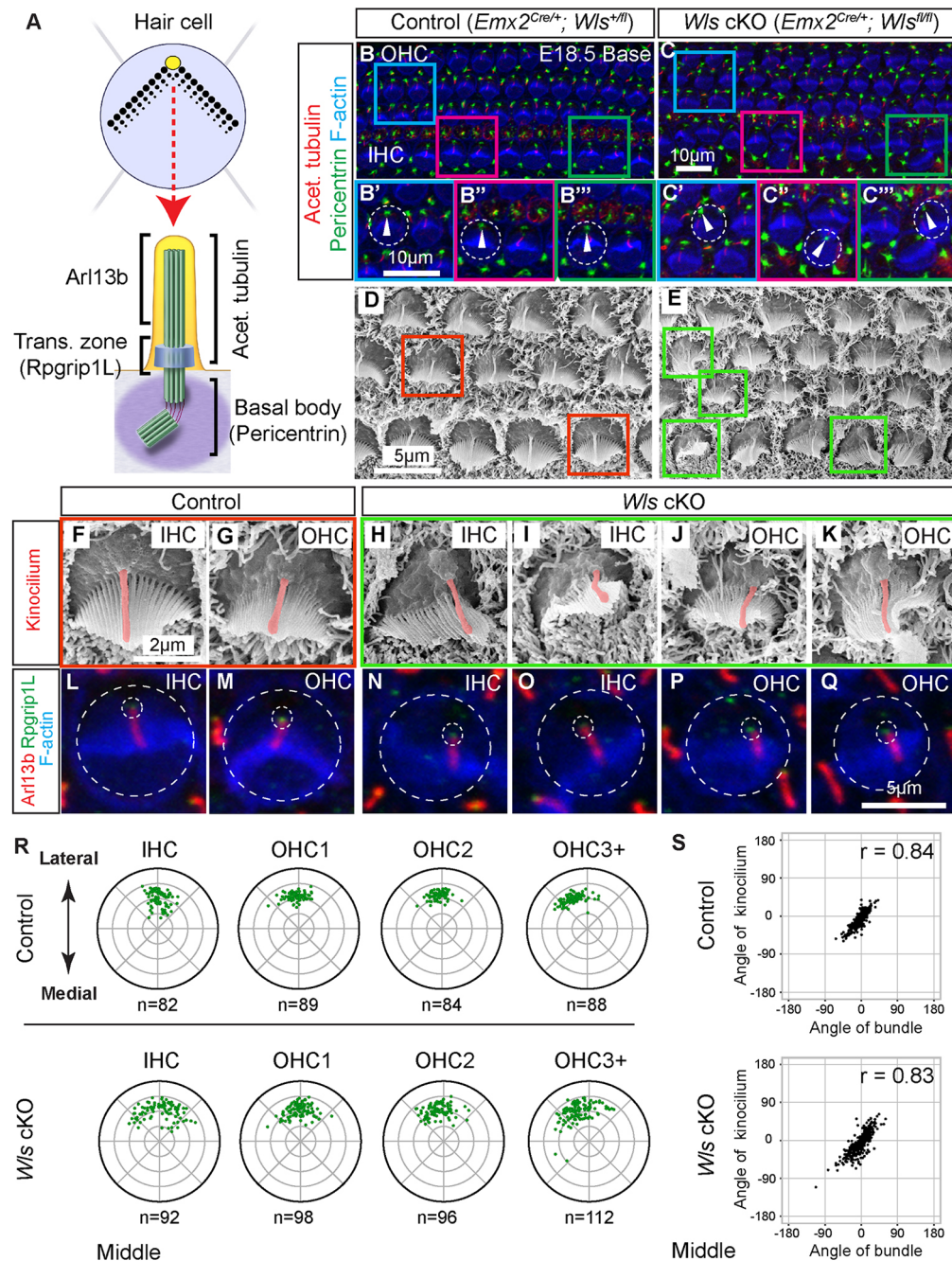


Fig. 4. Kinocilia positioning defects in *Wls* cKO cochlea. (A) A hair cell (HC), stereocilia bundles (green), kinocilium (yellow) and associated basal body. (B) HCs labeled for pericentrin, acetylated tubulin and F-actin. Whole-mount preparation of the basal turn of control cochlea showing localization of basal body and kinocilia to the lateral aspect of the HCs and immediately adjacent to the vertex of stereocilia bundle. (B'-B'') Higher-magnification images of outer and inner HCs. Dashed circles highlight HC boundaries and arrowheads indicate basal body positions. (C) In *Wls* cKO cochlea, a subset of OHCs and IHCs displayed mislocalized basal body and kinocilium (arrowheads), in addition to stereocilia bundle orientation defects. (C'-C'') Higher-magnification images of outer and inner HCs. Dashed circles highlight HC boundaries and arrowheads indicate basal body positions. (D,E) SEM images of the basal turn of E18.5 cochlea. In control HCs (D), the kinocilia are uniformly arranged in the lateral pole and in close proximity to the vertex of the tallest row of stereocilia bundles. By contrast, *Wls* cKO HCs (E) displayed mispositioned kinocilium and misoriented bundles. (F-K) High-magnification images of control (F,G; from red boxed areas in D) and *Wls* (H-K; from green boxed areas in E) cKO HCs with false-colored kinocilia (red). In *Wls* cKO HCs (H-K), kinocilia appeared off-centered and removed from the vertex of stereocilia bundles. (L-Q) High-magnification images of control (L,M) and *Wls* cKO (N-Q) HCs labeled for Arl13b, Rpgrip1L and F-actin. In control HCs (L,M), Arl13b and Rpgrip1L were localized near the stereocilia bundle vertex. In the *Wls* cKO cochlea (N-Q), Arl13b and Rpgrip1L appeared off-centered in misoriented OHCs and IHCs. Outer and inner dashed circles highlight the HC boundaries and kinocilia positions, respectively. (R) Scatter plots of kinocilia positions (based on Rpgrip1L expression) in control and *Wls* cKO cochlea. In HCs from control cochlea, kinocilia positions were tightly clustered at the lateral pole. Kinocilia positions appeared more scattered in *Wls* cKO HCs than in control cells, most notably among IHCs and the third row of OHCs. In the scatter plots, concentric circles indicate relative distance from the center of the apical surface of HCs. (S) Significant correlation between the angular position of kinocilium and the angle of stereocilia bundle orientation in both the control (Pearson_{circular} correlation test, $r=0.84$, $n=343$, $P<0.001$) and *Wls* cKO cochleae (Pearson_{circular} correlation test, $r=0.83$, $n=398$, $P<0.001$). n =HC number analyzed from three control and *Wls* cKO cochleae.

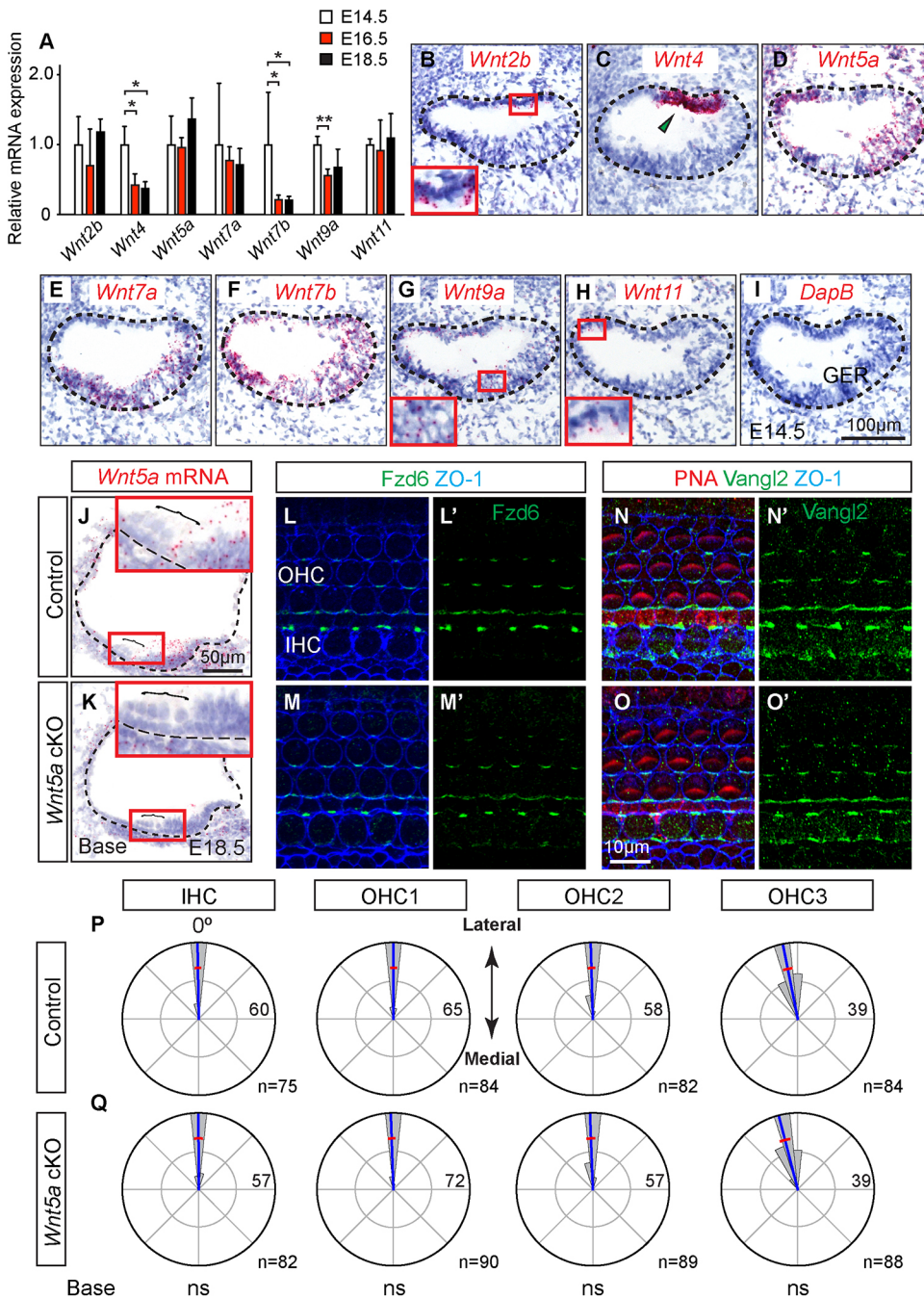


Fig. 5. Candidate Wnt ligands mediating planar cell polarity in the embryonic cochlea. (A) Detection of Wnt ligand expression in the cochlea by qPCR. *Wnt2b*, *Wnt4*, *Wnt5a*, *Wnt7a*, *Wnt7b*, *Wnt9a* and *Wnt11* mRNA in the cochlea from E14.5 to E18.5. *Wnt4* and *Wnt7b* expression were significantly lower at E16.5 and E18.5 than at E14.5. *Wnt9a* also decreased from E14.5 to E16.5. $n=3$ cochleae per age. (B-I) RNAscope *in situ* hybridization of E14.5 cochleae showing *Wnt2b*, *Wnt4* and *Wnt11* expression in the cochlear roof. In addition, *Wnt5a*, *Wnt7b* and *Wnt9a* expression was detected throughout the cochlear duct, whereas *Wnt7a* expression was seen in the cochlear floor. Insets are high-magnification images. *In situ* hybridization of each gene was performed on three independent wild-type cochleae. (J,K) *Wnt5a* expression was seen throughout the duct in control cochlea (J; *Emx2^{Cre/+}; Wnt5a^{+/fl}*). In contrast, cochlear duct of *Wnt5a* cKO embryos (K; *Emx2^{Cre/+}; Wnt5a^{fl/fl}*) showed a sharp decrease in *Wnt5a* mRNA signals. Insets are high-magnification images. The organ of Corti is marked by brackets. (L-O') Immunostaining shows Fz6 and Vangl2 enrichment in ZO1-marked tight junctions in control and *Wnt5a* cKO tissues. Stereocilia bundles are labeled with PNA. (P,Q) Rose plots showing the distribution of stereocilia bundle orientation in inner hair cells (IHCs) and outer hair cells (OHCs) in control and *Wnt5a* cKO cochleae. The length of each petal represents the number of HCs therein, with the number of the longest petal (also the radius of the outer circle) stated. When comparing individual rows of HCs, no significant differences in angle distribution were found between control and *Wnt5a* cKO cochleae (permutation test of equality of variances: IHC, $P=0.10$; OHC1, $P=0.90$; OHC2, $P=0.50$; OHC3, $P=0.7$). Zero degrees designates the mediolateral axis. Circular mean and circular s.d. are indicated with blue and red lines, respectively. $n=$ HC number analyzed from three control and *Wnt5a* cKO cochleae.

perturbing PCP molecules that remained asymmetrically localized in the *Wls* cKO cochleae would increase the severity of PCP defects. We used the mutant *Vangl2* model called Looptail (*Vangl2^{Lp}*), which is essential to planar polarization (Andre et al., 2012; Escobedo et al., 2013; Macheda et al., 2012; Saburi et al., 2012; Yamamoto et al., 2008). First, we analyzed *Wls* cKO animals in a *Vangl2^{Lp}* heterozygous background (*Wls* cKO; *Vangl2^{Lp/+}*) using *Emx2^{Cre/+}; Wls^{+/-}; Vangl2^{Lp/+}* as controls. In the basal turn of control cochleae, OHCs and IHCs showed no defects in planar polarization or kinocilium positioning (Fig. 6D,F, Fig. S13D,F), consistent with previous reports on *Vangl2^{Lp/+}* mice (Belotti et al., 2012). Relative to those in controls, stereocilia bundle orientation of each row of OHCs and IHCs in the *Wls* cKO; *Vangl2^{Lp/+}* cochlea was significantly more variable ($n=55$ control IHCs and 332 OHCs, and 106 *Wls* cKO; *Vangl2^{Lp/+}* IHCs and 402 OHCs, Fig. 6D-G,

Fig. S13D-G). Similarly, kinocilium positioning of each row of OHCs and IHCs in the *Wls* cKO; *Vangl2^{Lp/+}* cochlea was highly variable relative to those in controls, particularly in the OHC3+ group (Fig. 6F,G, Fig. S13F,G).

When comparing HCs between the *Wls* cKO and *Wls* cKO; *Vangl2^{Lp/+}* cochlea, the OHC3+ group from the latter showed significantly more variation in stereocilia bundle orientation (permutation test of equality of variances, $P<0.001$). In addition, the mean angle of stereocilia bundle orientation in the OHC3+ group was also significantly different between *Wls* cKO and *Wls* cKO; *Vangl2^{Lp/+}* cochleae (permutation test of equality of means, $P<0.001$). As the HC planar polarization defects in *Wls* cKO; *Vangl2^{Lp/+}* cochlea were worse than that in *Emx2^{Cre/+}; Wls^{+/-}; Vangl2^{Lp/+}* and *Wls* cKO cochleae, we postulate that Vangl2 and secreted Wnts co-regulate the polarization of HCs.

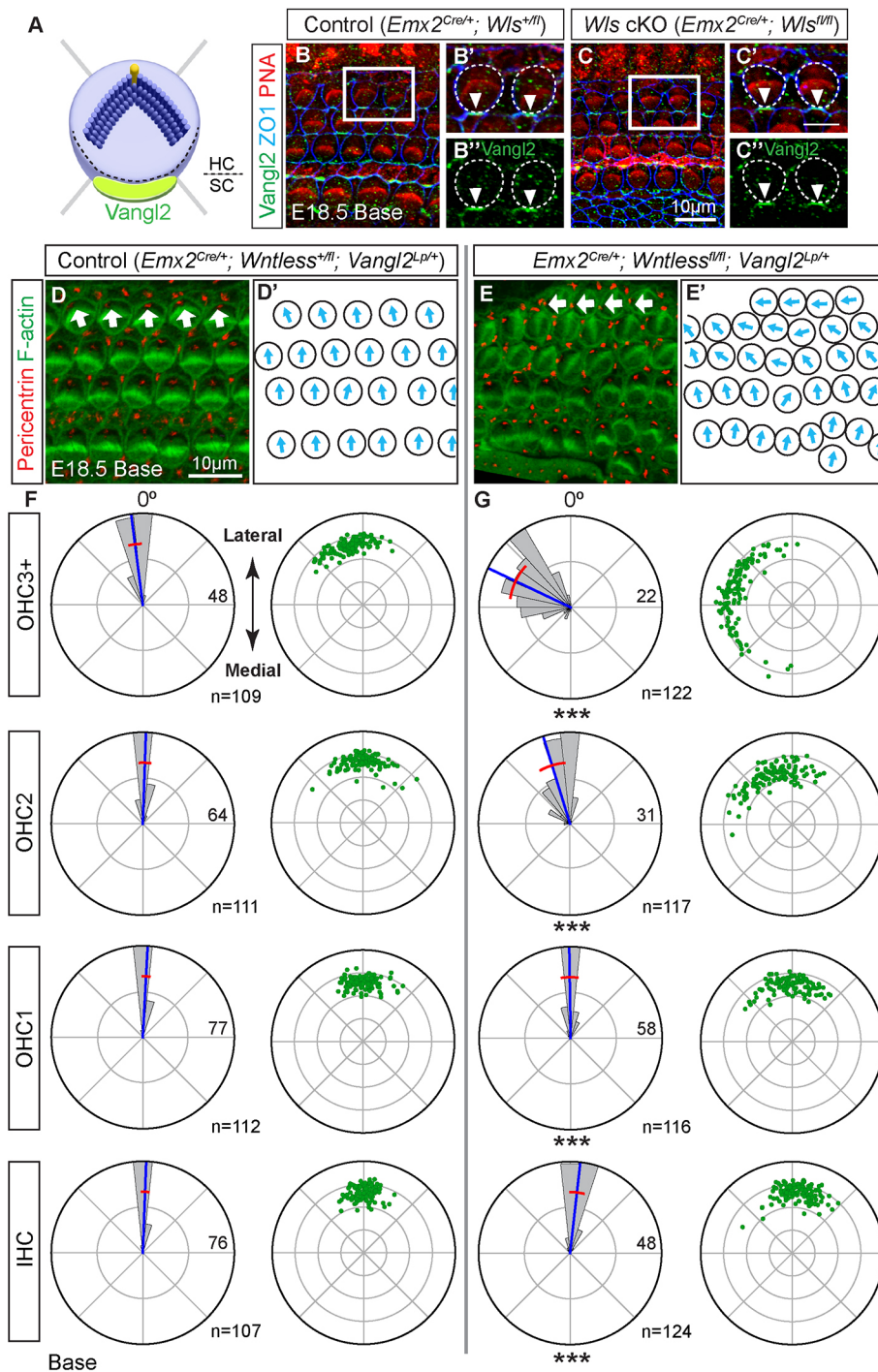


Fig. 6. *Vangl2* genetically interacts with *Wls* to regulate planar polarization. (A) Asymmetric localization of *Vangl2* at the lateral side of supporting cells. (B–C') Cochleae stained for *Vangl2* (arrowheads), tight junction protein ZO-1 and stereocilia bundles (PNA). Asymmetric localization of *Vangl2* was detected in both control and *Wls* cKO cochlea. B', B'', C', C'' show high-magnification images. Cell boundaries were outlined with dashed lines. (D, E) Whole-mount preparation of the basal turn stained for pericentrin and F-actin marking basal bodies and stereocilia bundles, respectively, in E18.5 control (D; *Emx2*^{Cre/+}; *Wls*^{+/fl}; *Vangl2*^{Lp/+}) and *Wls* cKO; *Vangl2*^{Lp/+} (E; *Emx2*^{Cre/+}; *Wls*^{fl/fl}; *Vangl2*^{Lp/+}) cochleae. In control tissues, normal bundle orientation and basal body positioning were observed. By contrast, *Wls* cKO; *Vangl2*^{Lp/+} tissues displayed misorientation of hair cell bundles and basal body positioning defects. In addition, *Wls* cKO; *Vangl2*^{Lp/+} cochlea exhibited extranumerary IHCs and OHCs, with the outermost row of OHCs displaying the most severe defects. Arrows indicate stereocilia bundle orientations. (D', E') The orientation of stereocilia bundles from individual hair cells in D, E, respectively. (F) Rose and scatter plots showing stereocilia bundle orientation and basal body (pericentrin) positioning, respectively. In control cochlea, bundles in each row of HCs were oriented along the mediolateral axis and kinocilia were tightly clustered at the lateral pole for IHCs and OHCs. (G) In *Wls* cKO; *Vangl2*^{Lp/+} cochlea, bundle orientations were significantly more variable and basal body positioning appeared more scattered than controls. These defects were most severe among the most lateral rows of OHCs. The mean angle of stereocilia bundle orientation between control and *Wls* cKO; *Vangl2*^{Lp/+} OHC3+ were significantly different (permutation test of equality of means, $P < 0.001$). The OHC3+ group included cells from OHC3 and OHCs located more laterally. In the rose plots, the blue and red lines indicate the circular mean and circular s.d., respectively. The length of each petal represents the number of hair cells therein, with the number of the longest petal (also the radius of the outer circle) stated. n = HC number analyzed from three control and *Wls* cKO; *Vangl2*^{Lp/+} cochleae. Zero degrees designate the mediolateral axis. Within rose diagrams, the radius of inner circle is half of that of the outer circle. In the scatter plots, concentric circles indicate relative distance from the center of the apical surface of HCs. Permutation test of equality of variances. *** $P < 0.001$.

Because the *Vangl2*^{Lp} allele has been reported to have a dominant-negative effect (Yin et al., 2012), we also conditionally deleted one copy of *Vangl2* allele from the cochlear duct by generating the *Emx2*^{Cre/+}; *Wls*^{fl/fl}; *Vangl2*^{fl/+} (*Wls* cKO; *Vangl2*^{fl/+}) animals using *Emx2*^{Cre/+}; *Wls*^{fl/+}; *Vangl2*^{fl/+} as controls (Fig. S14A–D). Similar to *Wls* cKO; *Vangl2*^{Lp/+} cochlea, *Wls* cKO; *Vangl2*^{fl/+} cochleae were widened with supernumerary IHCs and OHCs, both of which display severe defects in stereocilia bundle orientation and kinocilia positioning relative to littermate controls (Fig. S14A–D). Together, these experiments indicate that a decrease in *Vangl2* gene dose in a *Wls* cKO background is sufficient to accentuate HC orientation defects in the cochlea, further

supporting the notion that secreted Wnts and *Vangl2* coordinate to regulate HC polarization.

DISCUSSION

The critical role of PCP core proteins in regulating planar polarization in various organs is well conserved across multiple organisms. However, our understanding of the signals upstream of the PCP pathway and how they regulate PCP core proteins is rather limited. Although previous studies suggest that Wnt proteins can serve as polarity cues for PCP signaling (Chu and Sokol, 2016; Gros et al., 2009; Minegishi et al., 2017; Qian et al., 2007; Wu et al., 2013), phenotypes of PCP defects among Wnt mutants vary widely,

possibly because of functional redundancy among Wnt ligands. Here, we have used two independent transgenic mouse models to prevent Wnt secretion in the cochlear duct, and found that Wnt secretion is required for planar polarization of sensory HCs. Similar results were independently reported recently (Landin Malt et al., 2020). Although the severity of PCP defects was mild, using asymmetric localization of PCP proteins as a molecular read out, we revealed specific PCP proteins that lost asymmetry in HCs in the *Wls* cKO cochlea. Among the PCP core proteins that remained asymmetrically localized in the *Wls* cKO cochlea, we perturbed *Vangl2* using two mouse strains and found that the combination of *Wls* ablation and haploinsufficiency of *Vangl2* accentuated HC orientation defects relative to either deficiency alone. Based on these findings, we propose a dual-lock model where secreted Wnts and *Vangl2* cooperate to ensure proper HC polarization in the embryonic cochlea (Fig. 7).

Disruption of Wnt secretion and Wnt/ β -catenin signaling in the embryonic cochlea

Wnt signaling is classically divided into the Wnt/ β -catenin (or canonical) and PCP (or non-canonical) pathways (van Amerongen and Nusse, 2009). Here, we have characterized the effects of disrupting Wnt secretion in the PCP pathway context, yet manipulation of *Wls* and *Porcn* can also affect the Wnt/ β -catenin pathway. Depending on the spatiotemporal patterns of its deletion, β -catenin, the main mediator of the Wnt/ β -catenin pathway, serves different functions, including HC specification, HC differentiation, radial patterning of the cochlea, proliferation of prosensory cells, and also differentiation and proliferation of the periotic mesenchymal cells (Atkinson et al., 2018; Bohnenpoll et al., 2014; Groves and Fekete, 2012; Jansson et al., 2019; Munnamalai and Fekete, 2020;

Shi et al., 2014). The current study shows that ablation of *Wls* or *Porcn*, did not cause overt HC specification defects, suggesting that some levels of the Wnt/ β -catenin pathway remained present in these mutants. Moreover, whether radial patterning defects leading to subtle anomalous HC and supporting cell differentiation occur in the *Wls* and *Porcn* cKO cochlea is unknown. Assessing how Wnt secretion regulates activity of the Wnt/ β -catenin pathway, radially patterning and HC and supporting cell differentiation, and how the Wnt/ β -catenin and Wnt/PCP pathways relate to each other in the cochlear duct should be of interest in future studies.

Finally, we have attributed shortening of the *Wls* and *Porcn* cKO cochlea to convergent extension defects. However, it is also possible that shortening cochlea is in part caused by decreases in prosensory cell proliferation, which is dependent on Wnt signaling (Jacques et al., 2012). To test these possibilities, further studies are needed to study the mitotic state of prosensory cells and the analysis of HC and SC markers along the mediolateral axis in *Wls* and *Porcn* cKO cochlea.

In both the *Wls* and *Porcn* cKO models, ablation was spatially restricted to the cochlear duct (and spiral ganglia neurons for *Porcn*). Mice with earlier deletion of *Wls* (*Pax2-Cre; Wls^{fl/fl}*) failed to develop any cochlear structures, thereby preventing the analysis of hair cell specification. Considering that numerous Wnt members have been detected in the periotic mesenchyme, it is possible that more severe PCP phenotypes and HC specification defects could be observed by a broader and earlier deletion of *Porcn* and *Wls*. As we did not measure the levels of Wnt target genes, the *Wls* and *Porcn* cKO cochlea likely represent models with partial loss of Wnt signaling. Future experiments to more broadly ablate these two genes from the periotic mesenchyme should be considered.

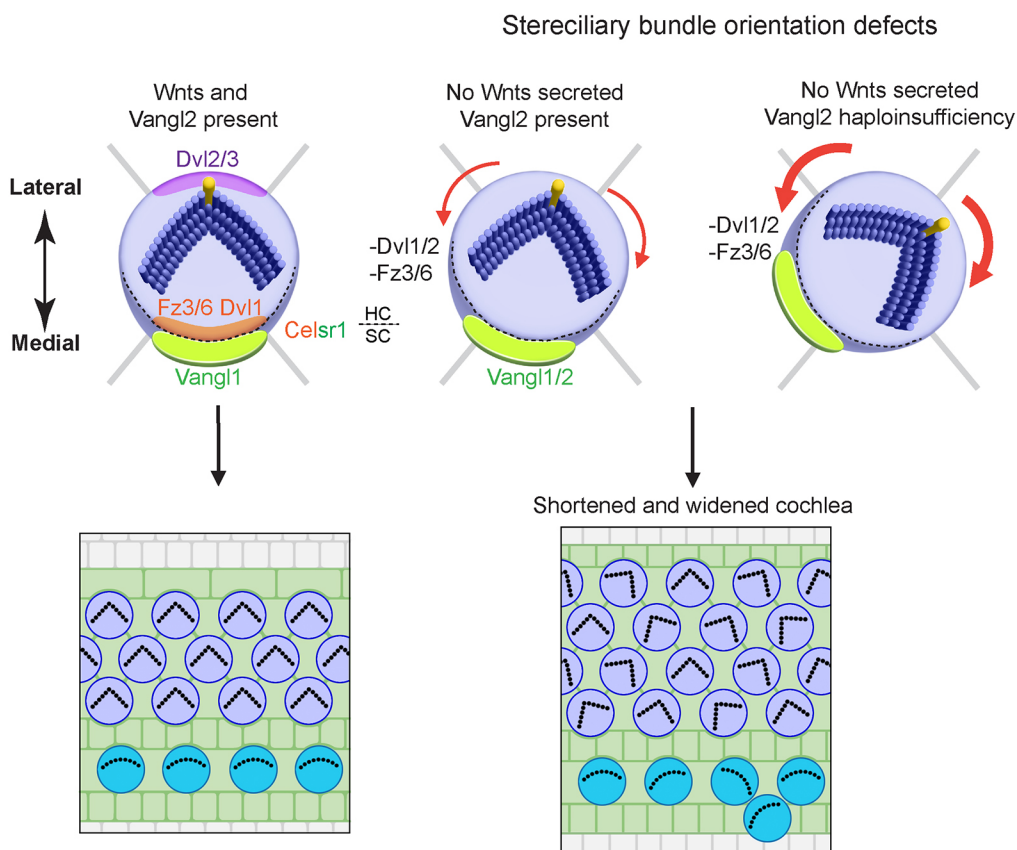


Fig. 7. Secreted Wnts and Vangl2 coordinate to regulate hair cell orientation. Proposed 'dual lock' model where secreted Wnts regulate the localization of Dvl1/2 and Fz3/6, which are important for cochlear extension and hair cell planar polarization in the developing cochlea. The absence of secreted Wnts 'loosens' the tightly regulated cell polarity, leading to relatively mild PCP defects. The combination of *Wls* deficiency in the cochlear duct and haploinsufficiency of *Vangl2* accentuates the PCP defects.

Wnt-dependent polarization of PCP proteins

PCP core proteins form complexes at cell junctions to regulate cell polarity. Their differential dependence on Wnt ligands first implicates Wnts as external cues directing PCP signaling, and also hints at the possible presence of other cues for Wnt-independent PCP signaling. For example, during mouse limb morphogenesis, FGF signaling is required for limb patterning in the proximal-distal axis while Wnt5a concurrently acts as a permissive signal (Gao et al., 2018). Moreover, protocadherins (Fat and Dachous) may also direct polarization of PCP core proteins in *Drosophila* wing epithelium and PCP-mediated neuronal migration in mice (Ma et al., 2003; Zakaria et al., 2014). Their exact roles in PCP remain unresolved and the approach of ablating the Wnt secretory pathway may help reveal their potential interplay with the Wnt-dependent PCP pathway.

Dishevelled proteins are important PCP components that function redundantly to regulate cochlear extension and stereocilia bundle orientation in the developing cochlea (Etheridge et al., 2008; Wang et al., 2006a). Our results indicate that localization of Dvl1 and Dvl2, but not Dvl3, is dependent on Wnt secretion. Similar to *Wls* and *Porcn* cKO cochleae, *Dvl1/Dvl2* double knockout (DKO) displayed frequent misalignment of HC stereocilia bundles (Etheridge et al., 2008; Wang et al., 2006a). On the other hand, *Dvl3* deficiency alone also cause mild PCP defects in the cochlea, suggesting divergent effects of Dvl members on planar polarization in addition to differing sensitivities to Wnt secretion. Although Dvl2 deficiency alone does not cause defects in HC planar polarization, it genetically interacts with Vangl2 as cochlea from *Dvl2^{-/-}; Vangl2^{Lp/Lp}* mice displays PCP defects (Wang et al., 2006a). This interaction supports the notion of a dual regulation by secreted Wnts and Vangl2.

Similarly, the transmembrane proteins Fz3 and Fz6 serve redundant function in the PCP pathway in the cochlea, with *Fz3/6* DKO, but not individual *Fz3* or *Fz6* KO animals, showing stereocilia bundle orientation defects (Wang et al., 2006b). While stereocilia bundle defects are typically more severe in OHCs among PCP mutants (Torban et al., 2008; Yin et al., 2012), IHCs in *Fz3/6* DKO animals displayed severe defects, whereas OHCs exhibited only modest defects in orientation and some disorganization (Wang et al., 2006b). These phenotypes more closely resemble those observed in *Wls* and *Porcn* cKO cochleae, where IHCs exhibited more prominent defects in stereocilia bundle orientation than OHCs. One possible explanation for this difference in severity is that mislocalized Fz3 and Fz6 still carried out partial function in the cochlea, or that mislocalized Fz proteins are more readily compensated for by other Fz members in the developing cochlea (Geng et al., 2016). In addition, given the fact that membrane localization of PCP core proteins is inter-dependent, e.g. Fz with Vangl2, the above arguments may also explain why some of the PCP core components remained polarized in the cochlea of *Wls* cKO animals.

Celsr1, Vangl1 and Vangl2 proteins have long been implicated in PCP in the developing mouse cochlear and vestibular systems (Curtin et al., 2003; Montcouquiol et al., 2003; Torban et al., 2008). During limb development, asymmetric localization of Vangl2 is lost in *Wnt5a^{-/-}* mice (Gao et al., 2011). Moreover, polarized localization of Vangl1, Pk2 and Celsr1 is impaired in node cells of *Wnt5a; Wnt5b* DKO embryos (Minegishi et al., 2017). On the other hand, in *Xenopus*, Wnt11b is required for Vangl2 polarization in the neural plate (Chu and Sokol, 2016). Although our study shows that the polarized localization of Celsr1, Vangl1 and Vangl2 are preserved in Wnt-deficient cochlea, we cannot rule out the possibility that post-translational modification of these proteins

occurs or that there is a subtle change in protein levels undetectable by our experimental approach. For example, a Wnt5a gradient can control PCP by inducing distinct levels of Vangl2 phosphorylation in the developing mouse limbs (Gao et al., 2011). Moreover, considering *Vangl2^{Lp/Lp}* mutants displayed mislocalization of Dvl2, Fz3 and Fz6 (Montcouquiol et al., 2006; Wang et al., 2006a,b), we do not rule out an interplay between Wnt-dependent PCP components and Vangl2.

Candidate Wnts regulating PCP signaling

Previous studies have demonstrated that *Porcn* and *Wls* are both indispensable for secretion of all Wnts across species, including mammals (Coudreuse and Korswagen, 2007; Nile and Hannoush, 2016; van den Heuvel et al., 1993). By ablating *Wls* and *Porcn* in the cochlear duct and characterizing expression of Wnt ligands therein, we have identified seven (*Wnt2b*, *Wnt4*, *Wnt5a*, *Wnt7a*, *Wnt7b*, *Wnt9a* and *Wnt11*) candidate Wnt genes that may individually or jointly direct PCP in this organ.

Our study shows that deletion of *Wnt5a* alone in the cochlear duct does not lead to PCP defects, which is in disagreement with results observed in *Wnt5a^{-/-}* embryos (Qian et al., 2007). It is important to point out that *Wnt5a* is also highly expressed outside the cochlear duct, and the role of extraductal sources of secreted Wnts was not directly examined. Alternatively, it is possible that germline deletion of *Wnt5a* leads to different phenotypes from *Wnt5a* cKOs.

Wnt ligands typically exert cellular effects over relatively short distances, Wnts expressed in the cochlear roof (*Wnt2b*, *Wnt4* and *Wnt11*) are presumably less likely to be governing HC planar polarization. Previous studies on *Wnt7a* and *Wnt9a* mutants reported no PCP defects in the cochlea (Dabdoub et al., 2003; Munnamalai et al., 2017). Interestingly, addition of Wnt7a protein or secreted Wnt antagonists to cultured cochlear explants caused defects in stereocilia bundle orientation in more laterally located OHCs (Dabdoub et al., 2003), suggesting that secreted Wnts may function to refine the orientation of OHCs. This is consistent with the concept that a Vangl2-independent mechanism governs stereociliary bundle refinement (Copley et al., 2013). Of note, we have detected both *Wnt7a* and *Wnt7b* in the cochlear floor (Fig. 5). It would be therefore informative to ablate these two genes, which may serve redundant functions in governing planar polarization (Cho et al., 2017).

When assessing planar polarization, severe defects such as those in mutants of PCP proteins are readily observed (Adler, 2012; Goodrich and Strutt, 2011; Singh and Mlodzik, 2012), whereas mutants of individual Wnts have been reported as normal or showing mild PCP defects (Wu et al., 2013). Numerous studies have successfully employed the use of the *Vangl2^{Lp}* mutants to accentuate a normal or mild PCP phenotype (Andre et al., 2012; Escobedo et al., 2013; Macheda et al., 2012; Saburi et al., 2012; Yamamoto et al., 2008). Here, we have shown that the loss of localized expression of Dvl1/2 and Fz3/6 may represent a molecular blueprint that aids the detection of mild PCP defects as a result of Wnt deficiency, an approach recently employed to explore mechanisms of Wnt-mediated HC polarization. Importantly, our results imply that regulation of PCP is more complex than previously appreciated. Such a redundancy in regulation ensures precise patterning of the cochlea, and should guide the investigation of how other complex organs are assembled.

MATERIALS AND METHODS

Mice

The following mouse strains were used: *Wls^{lox/lox}* (stock 012888) (Carpenter et al., 2010), *Vangl2^{lox/lox}* (stock 025174) (Copley et al.,

2013), *Vangl2^{Lp/+}* (stock 000220) (Strong and Hollander, 1949), *Wnt5a^{flox/flox}* (stock 026626) (Ryu et al., 2013) and *Rosa26^{tdTomato/+}* (stock 007909) (Madisen et al., 2010) (all obtained from the Jackson Laboratory), *Emx2^{cre/+}* (generated by S. Aizawa, RIKEN Center for Developmental Biology, Japan) (Kimura et al., 2005), *Porcn^{flox/flox}* (provided by I. B. Van den Veyver, Baylor University, TX, USA) (Liu et al., 2012) and *Pax2^{cre/+}* (provided by A. Groves, Baylor University, TX, USA) (Ohyama and Groves, 2004). The Animal Care and Use Committee of Stanford University School of Medicine approved all protocols.

Genotyping

DNA templates were generated by incubating mouse tail-tip biopsies in 50 mM NaOH at 98°C for 1 h followed by the addition of 30 µl of 1 M Tris-HCl (pH 8.0). We used either GoTaq or KAPA Taq PCR master mixes to amplify DNA fragments. The primers used were: *Wls-flox* (fwd, 5'-aggcttcgaactgaactgacc-3'; rev, 5'-ctcagaactccctcttgaagc-3'), *Vangl2-flox* (fwd, 5'-cagaatcctcctgtccctga-3'; rev, 5'-ctcagcctaaccacctctgc-3'), *Wnt5a-flox* (fwd, 5'-ggtgagactggaagtgc-3'; rev, 5'-ggagcagatgtttatgcctc-3'), *R26R-tdTomato* (fwd1, 5'-tgcccagactcatccttggc-3'; fwd2, 5'-ggcattaagcagcgtatcc-3'; rev1, 5'-ctgttcctgacggatgg-3'; rev2, 5'-aaggagctcagtgagta-3'), *Emx2-Cre* (fwd, 5'-gagtaaatgacgaccaatcaagcc-3'; rev1, 5'-cgaacatctcagg-ttctcggg-3'; rev2, 5'-cttggaaagcagatgaccagatcgg-3') and *Pax2-Cre* (fwd, 5'-cgatgcaacgagtgatgaggt-3'; rev, 5'-gcacgttcaccggcacaac-3'). *Vangl2^{Lp/+}* animals were genotyped by PCR amplification of a 228 bp fragment containing the S464N mutation, which was then digested with Hpy166II restriction enzyme as described previously (Vladar et al., 2012). The primers used were: *Vangl2^{Lp}* (fwd, 5'-atattgctgctggaccaccatcc-3'; rev, 5'-tgcagccgcatgacgaactatgta-3').

Quantitative PCR

Total RNA isolation from embryonic cochleae was carried out using RNeasy Extraction kit (Qiagen). A genomic DNA removal step was included in the workflow, as described in the manufacturer's instructions. Next, cDNA synthesis was performed using Superscript VILO Master Mix (Invitrogen) and qPCR reactions were carried out with SsoFast EvaGreen Supermix on a CFX96 real-time PCR system (BioRad). The $\Delta\Delta C_T$ method (Schmittgen and Livak, 2008) was used to analyze relative gene expression in samples using *Rpl19* as the endogenous reference gene. In our analysis, we only included genes whose expression was equal to or below a cut-off of 34 cycles, which approximately corresponded to a ΔC_T value of 14. All qPCR reactions were performed in triplicate in three or more independent biological replications. For a complete list of qPCR primers used, see Table S1. With the exception of *Wnt16*, all qPCR primers span an exon-exon boundary. In addition, individual pairs of primers were validated using cDNA libraries from a variety of mouse tissues expressing targets of interest (individual Wnts, *Wntless* and *Porcn*).

Immunohistochemistry

For cryosections, the otic capsule was removed and then fixed in 4% paraformaldehyde (PFA, Electron Microscopy Sciences) for 24 h at 4°C followed by short washes with PBS buffer. Tissues were then sequentially embedded in 10, 20 and 30% of sucrose diluted in PBS buffer and finally snap-frozen in 100% OCT (Sakura). Tissues were cut into 10–14 µm sections prior to immunohistochemistry. For whole-mount preparation, cochlear tissues were fixed in 4% PFA from 1 to 24 h (with duration dependent on the antigen of interest) at 4°C prior to incubation with primary antibodies overnight at 4°C. For other antigens (Fz6, Dvl2, Dvl3, *Vangl1*, *Vangl2* and *Wls*), we fixed cochlear tissues in 10% TCA on ice for 1 h. For a complete list of primary antibodies used in this study see Table S2. In addition, the secondary antibodies used in this study were conjugated to Alexa Fluor (488, 546 or 647) (ThermoFisher, 1:500). We also used fluorescent-conjugated phalloidin (Alexa 488, 546 or 647) to label F-actin (ThermoFisher, 1:500). Alternatively, peanut agglutinin (PNA) coupled to Alexa Fluor 647 was used to detect the stereocilia bundle (ThermoFisher). DAPI (ThermoFisher, 1:10,000) was used as a nuclear counterstain. After fixation and staining, tissues were micro-dissected and mounted in Prolong-

Gold. Control and cKO tissues were always processed and imaged in parallel.

Scanning electron microscopy (SEM)

Inner ears were isolated in washing buffer [0.05 mM HEPES buffer (pH 7.2), 10 mM CaCl₂, 5 mM MgCl₂, 0.9% NaCl] and fixed in 4% formaldehyde in washing buffer for 30 min at room temperature. The inner ears were then dissected to remove the stria vascularis, Reissner's and tectorial membranes. The samples were re-fixed in 2.5% glutaraldehyde, 4% formaldehyde in washing buffer overnight at 4°C, then washed extensively. The samples were dehydrated in ethanol (30%, 75%, 100% and 100%, 5 min incubation) and processed to critical drying point using an Autosamdri-815A (Tousimis). Cochleae were mounted on a stud with silver paint and coated with 5 nm of Iridium (sputter coater EMS150TS; Electron Microscopy Sciences). Samples were imaged at 5 kV with a FEI Magellan 400 XHR Field Emission Scanning Electron Microscope at the Stanford Nano Shared Facilities.

In situ hybridization

Harvested tissues were fixed in 4% PFA overnight at 4°C, embedded for cryosections and prepared as 10 µm sections as described above. RNAScope and BaseScope were performed as follows: tissue sections were hybridized with commercial probes from Advanced Cell Diagnostics (ACDbio) and counterstained with Hematoxylin (Sigma-Aldrich) according to the manufacturer's instructions for fixed frozen sections with colorimetric detection. Briefly, sections were washed in PBS (1×) for 5 min and then treated with H₂O₂ for 10 min. Next, sections were permeabilized using target retrieval reagent (ACDbio) and proteinase before hybridization. Probes used were: *DapB* (310043), *Polr2a* (310451), *Wls* (405011), *Porcn* (404971), *Porcn_E3_E7* (433251), *Atoh1* (408791), *Wnt2b* (405031), *Wnt4* (401101), *Wnt5a* (316791), *Wnt5a_2EJ* (717251), *Wnt7a* (401121), *Wnt7b* (401131), *Wnt9a* (405081) and *Wnt11* (405021) (all from Advanced Cell Diagnostics). Control and cKO cochleae were processed in parallel, with sections collected on the same slide and subjected to mRNA detection under identical conditions.

Image capture and analyses

Fluorescence-labeled images were acquired using a Zeiss LSM700 confocal microscope. *In situ* hybridized sections were imaged using an Axioplan 2 microscope coupled to a MRC5 (bright field) camera and using Axiovision AC software (Release 4.8, Carl Zeiss). Further imaging processing was carried out using Photoshop CS6 (Adobe Systems) and image analysis was performed using ImageJ (NIH).

Hair bundle orientation and kinocilia/basal body measurements

The organ of Corti was imaged by confocal microscopy at the basal and middle turns. Prior to quantification, we oriented the confocal images such that the apical-basal axis goes from left to right of the image, whereas outer hair cells and inner hair cells are positioned at the top and bottom of the image, respectively. Measurements of stereocilia bundle orientation and kinocilia/basal body position in hair cells were acquired using a custom Python program. First, z-stack confocal images of the organ of Corti were uploaded into the program. Second, through sequential selections, individual hair cells were outlined, and then stereocilia bundle and kinocilia/basal body angles were calculated with respect to the mediolateral axis of the organ of Corti, and a reference line drawn parallel to the pillar cells. Once hair cells in the image were selected, the measurements were saved as a csv file. Data points from these csv files were then plotted using custom Python scripts. The circular mean and circular standard deviations for each dataset were calculated using SciPy. All the scripts used in this article can be found in <https://github.com/a-jacobov/Cell-Polarity-Measurements>.

Statistics

Statistical analyses were conducted using Excel (Microsoft) and Prism 7 (GraphPad) software. Two-tailed, unpaired Student's *t*-test was used. *P* < 0.05 was considered significant. In addition, we tested for equality of

means and variance using a permutation test (also called a randomization test) (Ernst, 2004) with a Monte Carlo estimate of the *P*-values. This method allows no prior assumptions on the distribution of orientation. To gain greater statistical power, we sampled $B=10,000$ permutations, considering each mouse as a sampling unit, and compared the difference in means between control and mutant mice and the difference in variances. Details of the R code for permutation test are included in the supplementary Materials and Methods. Circular correlation analysis was performed using the R package ‘circular’. In short, the cor.circular function calculates the circular version of Pearson’s product moment correlation for two linear variables *X* and *Y*. The outputs also include the test statistics and a *P* value. $P<0.05$ was considered significant. The R package ‘circular’ can be found in <https://www.rdocumentation.org/packages/circular>. Data are shown as mean \pm s.d.

Acknowledgements

We thank J. Axelrod and our laboratory for insightful comments on the manuscript, W. Dong, T. Jan, J. Chang, P. Minhas and A. Rajan for excellent technical support, C. Sabatti for statistical assistance, I. B. Van den Veyver for sharing *Porcn*^{+/fl} mice, S. Aizawa for *Emx2-Cre* mice, E. Fuchs for *Celsr1* antibodies, Q. Du for LGN antibodies, and J. Nathans for Fz3 antibodies.

Competing interests

The authors declare no competing or financial interests.

Author contributions

Conceptualization: A.G.C., E.H.N.; Methodology: A.G.C., E.H.N., N.G.; Software: A.J.; Validation: E.H.N., N.G.; Formal analysis: A.G.C., E.H.N., N.G.; Investigation: E.H.N., N.G., A.J., J.H., L.A.Q.; Resources: E.H.N.; Writing - original draft: A.G.C., E.H.N.; Writing - review & editing: A.G.C., E.H.N., N.G., A.J., J.H., L.A.Q.; Supervision: A.G.C.; Project administration: A.G.C.; Funding acquisition: A.G.C., E.H.N., N.G.

Funding

This work was supported by Lucile Packard Foundation for Stanford Children’s Health (NIH-NCATS-CTSA UL1TR001085), by the Child Health Research Institute of Stanford University and by the National Institutes of Health/National Institute on Deafness and Other Communication Disorders (F32DC14623) (all to E.H.N.); by a Stanford Nano Shared Facilities Seed Grant and by the National Institutes of Health/National Institute on Deafness and Other Communication Disorders (RO1DC016409) (both to N.G.); and by the National Institutes of Health/National Institute on Deafness and Other Communication Disorders (RO1DC01910), by the Akiko Yamazaki and Jerry Yang Faculty Scholar Fund, by the California Initiative in Regenerative Medicine (RN3-06529), and by the Yu and Oberndorf families (all to A.G.C.). Deposited in PMC for release after 12 months.

Supplementary information

Supplementary information available online at <https://dev.biologists.org/lookup/doi/10.1242/dev.191981.supplemental>

Peer review history

The peer review history is available online at <https://dev.biologists.org/lookup/doi/10.1242/dev.191981.viewer-comments.pdf>

References

Adler, P. N. (2012). The frizzled/stan pathway and planar cell polarity in the *Drosophila* wing. *Curr. Top. Dev. Biol.* **101**, 1-31. doi:10.1016/B978-0-12-394592-1.00001-6

Andre, P., Wang, Q., Wang, N., Gao, B., Schilit, A., Halford, M. M., Stacker, S. A., Zhang, X. and Yang, Y. (2012). The Wnt coreceptor Ryk regulates Wnt/planar cell polarity by modulating the degradation of the core planar cell polarity component Vangl2. *J. Biol. Chem.* **287**, 44518-44525. doi:10.1074/jbc.M112.414441

Atkinson, P. J., Dong, Y., Gu, S., Liu, W., Najarro, E. H., Udagawa, T. and Cheng, A. G. (2018). Sox2 haploinsufficiency primes regeneration and Wnt responsiveness in the mouse cochlea. *J. Clin. Invest.* **128**, 1641-1656. doi:10.1172/JCI97248

Bänziger, C., Soldini, D., Schütt, C., Zipperlen, P., Hausmann, G. and Basler, K. (2006). Wntless, a conserved membrane protein dedicated to the secretion of Wnt proteins from signaling cells. *Cell* **125**, 509-522. doi:10.1016/j.cell.2006.02.049

Barrott, J. J., Cash, G. M., Smith, A. P., Barrow, J. R. and Murtaugh, L. C. (2011). Deletion of mouse *Porcn* blocks Wnt ligand secretion and reveals an ectodermal etiology of human focal dermal hypoplasia/Goltz syndrome. *Proc. Natl. Acad. Sci. USA* **108**, 12752-12757. doi:10.1073/pnas.1006437108

Bartscherer, K., Pelte, N., Ingelfinger, D. and Boutros, M. (2006). Secretion of Wnt ligands requires Evi, a conserved transmembrane protein. *Cell* **125**, 523-533. doi:10.1016/j.cell.2006.04.009

Basch, M. L., Brown, R. M., II, Jen, H.-I. and Groves, A. K. (2016). Where hearing starts: the development of the mammalian cochlea. *J. Anat.* **228**, 233-254. doi:10.1111/joa.12314

Belotti, E., Puvirajesinghe, T. M., Audebert, S., Baudelet, E., Camoin, L., Pierres, M., Lasvaux, L., Ferracci, G., Montcouquiou, M. and Borg, J.-P. (2012). Molecular characterisation of endogenous Vangl2/Vangl1 heteromeric protein complexes. *PLoS ONE* **7**, e46213. doi:10.1371/journal.pone.0046213

Biechele, S., Adissu, H. A., Cox, B. J. and Rossant, J. (2013). Zygotic *Porcn* paternal allele deletion in mice to model human focal dermal hypoplasia. *PLoS ONE* **8**, e79139. doi:10.1371/journal.pone.0079139

Bohnenpoll, T., Trowe, M.-O., Wojahn, I., Taketo, M. M., Petry, M. and Kispert, A. (2014). Canonical Wnt signaling regulates the proliferative expansion and differentiation of fibrocytes in the murine inner ear. *Dev. Biol.* **391**, 54-65. doi:10.1016/j.ydbio.2014.03.023

Butler, M. T. and Wallingford, J. B. (2017). Planar cell polarity in development and disease. *Nat. Rev. Mol. Cell Biol.* **18**, 375-388. doi:10.1038/nrm.2017.11

Carpenter, A. C., Rao, S., Wells, J. M., Campbell, K. and Lang, R. A. (2010). Generation of mice with a conditional null allele for Wntless. *Genesis* **48**, 554-558. doi:10.1002/dvg.20651

Carpenter, A. C., Smith, A. N., Wagner, H., Cohen-Tayar, Y., Rao, S., Wallace, V., Ashery-Padan, R. and Lang, R. A. (2015). Wnt ligands from the embryonic surface ectoderm regulate ‘bimetallic strip’ optic cup morphogenesis in mouse. *Development* **142**, 972-982. doi:10.1242/dev.120022

Chacon-Heszele, M. F., Ren, D., Reynolds, A. B., Chi, F. and Chen, P. (2012). Regulation of cochlear convergent extension by the vertebrate planar cell polarity pathway is dependent on p120-catenin. *Development* **139**, 968-978. doi:10.1242/dev.065326

Cho, C., Smallwood, P. M. and Nathans, J. (2017). Reck and Gpr124 are essential receptor cofactors for Wnt7a/Wnt7b-specific signaling in mammalian CNS angiogenesis and blood-brain barrier regulation. *Neuron* **95**, 1221-1225. doi:10.1016/j.neuron.2017.08.032

Chu, C.-W. and Sokol, S. Y. (2016). Wnt proteins can direct planar cell polarity in vertebrate ectoderm. *eLife* **5**, e16463. doi:10.7554/eLife.16463

Copley, C. O., Duncan, J. S., Liu, C., Cheng, H. and Deans, M. R. (2013). Postnatal refinement of auditory hair cell planar polarity deficits occurs in the absence of Vangl2. *J. Neurosci.* **33**, 14001-14016. doi:10.1523/JNEUROSCI.1307-13.2013

Coudreuse, D. and Korswagen, H. C. (2007). The making of Wnt: new insights into Wnt maturation, sorting and secretion. *Development* **134**, 3-12. doi:10.1242/dev.02699

Curtin, J. A., Quint, E., Tsipouri, V., Arkell, R. M., Cattanch, B., Copp, A. J., Henderson, D. J., Spurr, N., Stanier, P., Fisher, E. M. et al. (2003). Mutation of *Celsr1* disrupts planar polarity of inner ear hair cells and causes severe neural tube defects in the mouse. *Curr. Biol.* **13**, 1129-1133. doi:10.1016/S0960-9822(03)00374-9

Dabdoub, A., Donohue, M. J., Brennan, A., Wolf, V., Montcouquiou, M., Sassoon, D. A., Hseih, J.-C., Rubin, J. S., Salinas, P. C. and Kelley, M. W. (2003). Wnt signaling mediates reorientation of outer hair cell stereociliary bundles in the mammalian cochlea. *Development* **130**, 2375-2384. doi:10.1242/dev.00448

Duncan, J. S., Stoller, M. L., Francl, A. F., Tissir, F., Devenport, D. and Deans, M. R. (2017). *Celsr1* coordinates the planar polarity of vestibular hair cells during inner ear development. *Dev. Biol.* **423**, 126-137. doi:10.1016/j.ydbio.2017.01.020

Ernst, M. D. (2004). Permutation methods: a basis for exact inference. *Stat. Sci.* **19**, 676-685. doi:10.1214/088342304000000396

Escobedo, N., Contreras, O., Munoz, R., Farias, M., Carrasco, H., Hill, C., Tran, U., Pryor, S. E., Wessely, O., Copp, A. J. et al. (2013). Syndecan 4 interacts genetically with Vangl2 to regulate neural tube closure and planar cell polarity. *Development* **140**, 3008-3017. doi:10.1242/dev.091173

Etheridge, S. L., Ray, S., Li, S., Hamblet, N. S., Lijam, N., Tsang, M., Greer, J., Kardos, N., Wang, J., Sussman, D. J. et al. (2008). Murine dishevelled 3 functions in redundant pathways with dishevelled 1 and 2 in normal cardiac outflow tract, cochlea, and neural tube development. *PLoS Genet.* **4**, e1000259. doi:10.1371/journal.pgen.1000259

Ezan, J., Lasvaux, L., Gezer, A., Novakovic, A., May-Simera, H., Belotti, E., Lhoumeau, A. C., Birnbaumer, L., Beer-Hammer, S., Borg, J. P. et al. (2013). Primary cilium migration depends on G-protein signalling control of subapical cytoskeleton. *Nat. Cell Biol.* **15**, 1107-1115. doi:10.1038/ncb2819

Gao, B., Song, H., Bishop, K., Elliot, G., Garrett, L., English, M. A., Andre, P., Robinson, J., Sood, R., Minami, Y. et al. (2011). Wnt signaling gradients establish planar cell polarity by inducing Vangl2 phosphorylation through Ror2. *Dev. Cell* **20**, 163-176. doi:10.1016/j.devcel.2011.01.001

Gao, B., Ajima, R., Yang, W., Li, C., Song, H., Anderson, M. J., Liu, R. R., Lewandoski, M. B., Yamaguchi, T. P. and Yang, Y. (2018). Coordinated directional outgrowth and pattern formation by integration of Wnt5a and Fgf signaling in planar cell polarity. *Development* **145**, dev163824. doi:10.1242/dev.163824

Geng, R., Noda, T., Mulvaney, J. F., Lin, V. Y. W., Edge, A. S. B. and Dabdoub, A. (2016). Comprehensive expression of Wnt signaling pathway genes during

- development and maturation of the mouse cochlea. *PLoS ONE* **11**, e0148339. doi:10.1371/journal.pone.0148339
- Ghimire, S. R. and Deans, M. R.** (2019). Frizzled3 and Frizzled6 cooperate with Vangl2 to direct cochlear innervation by type II spiral ganglion neurons. *J. Neurosci.* **39**, 8013-8023. doi:10.1523/JNEUROSCI.1740-19.2019
- Goodrich, L. V. and Strutt, D.** (2011). Principles of planar polarity in animal development. *Development* **138**, 1877-1892. doi:10.1242/dev.054080
- Gros, J., Serralbo, O. and Marcelle, C.** (2009). WNT11 acts as a directional cue to organize the elongation of early muscle fibres. *Nature* **457**, 589-593. doi:10.1038/nature07564
- Groves, A. K. and Fekete, D. M.** (2012). Shaping sound in space: the regulation of inner ear patterning. *Development* **139**, 245-257. doi:10.1242/dev.067074
- Herr, P., Hausmann, G. and Basler, K.** (2012). WNT secretion and signalling in human disease. *Trends Mol. Med.* **18**, 483-493. doi:10.1016/j.molmed.2012.06.008
- Jacques, B. E., Pulgilla, C., Weichert, R. M., Ferrer-Vaquer, A., Hadjantonakis, A.-K., Kelley, M. W. and Dabdoub, A.** (2012). A dual function for canonical Wnt/ β -catenin signaling in the developing mammalian cochlea. *Development* **139**, 4395-4404. doi:10.1242/dev.080358
- Jansson, L., Ebeid, M., Shen, J. W., Mokhtari, T. E., Quiruz, L. A., Ornitz, D. M., Huh, S.-H. and Cheng, A. G.** (2019). β -Catenin is required for radial cell patterning and identity in the developing mouse cochlea. *Proc. Natl. Acad. Sci. USA* **116**, 21054-21060. doi:10.1073/pnas.1910223116
- Jiang, M., Ku, W.-Y., Fu, J., Offermanns, S., Hsu, W. and Que, J.** (2013). Gpr177 regulates pulmonary vasculature development. *Development* **140**, 3589-3594. doi:10.1242/dev.095471
- Jones, C., Qian, D., Kim, S. M., Li, S., Ren, D., Knapp, L., Sprinzak, D., Avraham, K. B., Matsuzaki, F., Chi, F. et al.** (2014). Ankrd6 is a mammalian functional homolog of *Drosophila* planar cell polarity gene *disco* and regulates coordinated cellular orientation in the mouse inner ear. *Dev. Biol.* **395**, 62-72. doi:10.1016/j.ydbio.2014.08.029
- Kadowaki, T., Wilder, E., Klingensmith, J., Zachary, K. and Perrimon, N.** (1996). The segment polarity gene *porcupine* encodes a putative multitransmembrane protein involved in Wingless processing. *Genes Dev.* **10**, 3116-3128. doi:10.1101/gad.10.24.3116
- Kilian, B., Mansukoski, H., Barbosa, F. C., Ulrich, F., Tada, M. and Heisenberg, C.-P.** (2003). The role of Ppt/Wnt5 in regulating cell shape and movement during zebrafish gastrulation. *Mech. Dev.* **120**, 467-476. doi:10.1016/S0925-4773(03)00004-2
- Kimura, J., Suda, Y., Kurokawa, D., Hossain, Z. M., Nakamura, M., Takahashi, M., Hara, A. and Aizawa, S.** (2005). *Emx2* and *Pax6* function in cooperation with *Otx2* and *Otx1* to develop caudal forebrain primordium that includes future archipallium. *J. Neurosci.* **25**, 5097-5108. doi:10.1523/JNEUROSCI.0239-05.2005
- Landin Malt, A., Hogan, A. K., Smith, C. D., Madani, M.S. and Lu, X.** (2020). Wnts regulate planar cell polarity via heterotrimeric G protein and PI3K signaling. *J. Cell Biol.* **219**, e201912071. doi:10.1083/jcb.201912071
- Liu, W., Shaver, T. M., Balasa, A., Ljungberg, M. C., Wang, X., Wen, S., Nguyen, H. and Van den Veyver, I. B.** (2012). Deletion of *Porcn* in mice leads to multiple developmental defects and models human focal dermal hypoplasia (Goltz syndrome). *PLoS ONE* **7**, e32331. doi:10.1371/journal.pone.0032331
- Ma, D., Yang, C.-H., McNeill, H., Simon, M. A. and Axelrod, J. D.** (2003). Fidelity in planar cell polarity signalling. *Nature* **421**, 543-547. doi:10.1038/nature01366
- Macheda, M. L., Sun, W. W., Kugathasan, K., Hogan, B. M., Bower, N. I., Halford, M. M., Zhang, Y. F., Jacques, B. E., Lieschke, G. J., Dabdoub, A. et al.** (2012). The Wnt receptor *Ryk* plays a role in mammalian planar cell polarity signaling. *J. Biol. Chem.* **287**, 29312-29323. doi:10.1074/jbc.M112.362681
- Madisen, L., Zwingman, T. A., Sunkin, S. M., Oh, S. W., Zariwala, H. A., Gu, H., Ng, L. L., Palmiter, R. D., Hawrylycz, M. J., Jones, A. R. et al.** (2010). A robust and high-throughput Cre reporting and characterization system for the whole mouse brain. *Nat. Neurosci.* **13**, 133-140. doi:10.1038/nn.2467
- May-Simera, H.** (2016). Evaluation of planar-cell-polarity phenotypes in ciliopathy mouse mutant cochlea. *J. Vis. Exp.* **108**, e53559. doi:10.3791/53559
- May-Simera, H. and Kelley, M. W.** (2012). Examining planar cell polarity in the mammalian cochlea. *Methods Mol. Biol.* **839**, 157-171. doi:10.1007/978-1-61779-510-7_13
- Merks, A. M., Swinarski, M., Meyer, A. M., Müller, N. V., Özcan, I., Donat, S., Burger, A., Gilbert, S., Mosimann, C., Abdellah-Seyfried, S. et al.** (2018). Planar cell polarity signalling coordinates heart tube remodelling through tissue-scale polarisation of actomyosin activity. *Nat. Commun.* **9**, 2161. doi:10.1038/s41467-018-04566-1
- Minogishi, K., Hashimoto, M., Ajima, R., Takaoka, K., Shinohara, K., Ikawa, Y., Nishimura, H., McMahan, A. P., Willert, K., Okada, Y. et al.** (2017). A Wnt5 activity asymmetry and intercellular signaling via PCP proteins polarize node cells for left-right symmetry breaking. *Dev. Cell* **40**, 439-452.e434. doi:10.1016/j.devcel.2017.02.010
- Montcouquiol, M., Rachel, R. A., Lanford, P. J., Copeland, N. G., Jenkins, N. A. and Kelley, M. W.** (2003). Identification of *Vangl2* and *Scrb1* as planar polarity genes in mammals. *Nature* **423**, 173-177. doi:10.1038/nature01618
- Montcouquiol, M., Sans, N., Huss, D., Kach, J., Dickman, J. D., Forge, A., Rachel, R. A., Copeland, N. G., Jenkins, N. A., Bogani, D. et al.** (2006). Asymmetric localization of *Vangl2* and *Fz3* indicate novel mechanisms for planar cell polarity in mammals. *J. Neurosci.* **26**, 5265-5275. doi:10.1523/JNEUROSCI.4680-05.2006
- Munnmalai, V. and Fekete, D. M.** (2020). The acquisition of positional information across the radial axis of the cochlea. *Dev. Dyn.* **249**, 281-297. doi:10.1002/dvdy.118
- Munnmalai, V., Sienknecht, U. J., Duncan, R. K., Scott, M. K., Thawani, A., Fantetti, K. N., Atallah, N. M., Biesemeier, D. J., Song, K. H., Luethy, K. et al.** (2017). *Wnt9a* can influence cell fates and neural connectivity across the radial axis of the developing cochlea. *J. Neurosci.* **37**, 8975-8988. doi:10.1523/JNEUROSCI.1554-17.2017
- Nile, A. H. and Hannoush, R. N.** (2016). Fatty acylation of Wnt proteins. *Nat. Chem. Biol.* **12**, 60-69. doi:10.1038/nchembio.2005
- Ohyama, T. and Groves, A. K.** (2004). Generation of *Pax2-Cre* mice by modification of a *Pax2* bacterial artificial chromosome. *Genesis* **38**, 195-199. doi:10.1002/gene.20017
- Ono, K., Kita, T., Sato, S., O'Neill, P., Mak, S.-S., Paschaki, M., Ito, M., Gotoh, N., Kawakami, K., Sasai, Y. et al.** (2014). *FGFR1-Frs2/3* signalling maintains sensory progenitors during inner ear hair cell formation. *PLoS Genet.* **10**, e1004118. doi:10.1371/journal.pgen.1004118
- Qian, D., Jones, C., Rzdzinska, A., Mark, S., Zhang, X., Steel, K. P., Dai, X. and Chen, P.** (2007). *Wnt5a* functions in planar cell polarity regulation in mice. *Dev. Biol.* **306**, 121-133. doi:10.1016/j.ydbio.2007.03.011
- Rida, P. C. G. and Chen, P.** (2009). Line up and listen: planar cell polarity regulation in the mammalian inner ear. *Semin. Cell Dev. Biol.* **20**, 978-985. doi:10.1016/j.semcdb.2009.02.007
- Rios-Esteves, J., Haugen, B. and Resh, M. D.** (2014). Identification of key residues and regions important for porcupine-mediated Wnt acylation. *J. Biol. Chem.* **289**, 17009-17019. doi:10.1074/jbc.M114.561209
- Ryu, Y. K., Collins, S. E., Ho, H.-Y. H., Zhao, H. and Kuruvilla, R.** (2013). An autocrine *Wnt5a-Ror* signaling loop mediates sympathetic target innervation. *Dev. Biol.* **377**, 79-89. doi:10.1016/j.ydbio.2013.02.013
- Saburi, S., Hester, I., Goodrich, L. and McNeill, H.** (2012). Functional interactions between *Fat* family cadherins in tissue morphogenesis and planar polarity. *Development* **139**, 1806-1820. doi:10.1242/dev.077461
- Schmittgen, T. D. and Livak, K. J.** (2008). Analyzing real-time PCR data by the comparative *C_T* method. *Nat. Protoc.* **3**, 1101-1108. doi:10.1038/nprot.2008.73
- Shi, F., Hu, L., Jacques, B. E., Mulvaney, J. F., Dabdoub, A. and Edge, A. S. B.** (2014). β -Catenin is required for hair-cell differentiation in the cochlea. *J. Neurosci.* **34**, 6470-6479. doi:10.1523/JNEUROSCI.4305-13.2014
- Simons, M. and Mlodzik, M.** (2008). Planar cell polarity signaling: from fly development to human disease. *Annu. Rev. Genet.* **42**, 517-540. doi:10.1146/annurev.genet.42.110807.091432
- Singh, J. and Mlodzik, M.** (2012). Planar cell polarity signaling: coordination of cellular orientation across tissues. *Wiley Interdiscipl. Rev. Dev. Biol.* **1**, 479-499. doi:10.1002/wdev.32
- Snowball, J., Ambalavanan, M., Whitsett, J. and Sinner, D.** (2015). Endodermal Wnt signaling is required for tracheal cartilage formation. *Dev. Biol.* **405**, 56-70. doi:10.1016/j.ydbio.2015.06.009
- Strong, L. C. and Hollander, W. F.** (1949). Hereditary loop-tail in the house mouse: accompanied by imperforate vagina and with lethal craniorachischisis when homozygous. *J. Hered.* **40**, 329-334. doi:10.1093/oxfordjournals.jhered.a105976
- Tarchini, B., Jolicoeur, C. and Cayouette, M.** (2013). A molecular blueprint at the apical surface establishes planar asymmetry in cochlear hair cells. *Dev. Cell* **27**, 88-102. doi:10.1016/j.devcel.2013.09.011
- Torban, E., Patenaude, A.-M., Leclerc, S., Rakowiecki, S., Gauthier, S., Andelfinger, G., Epstein, D. J. and Gros, P.** (2008). Genetic interaction between members of the *Vangl* family causes neural tube defects in mice. *Proc. Natl. Acad. Sci. USA* **105**, 3449-3454. doi:10.1073/pnas.0712126105
- van Amerongen, R. and Nusse, R.** (2009). Towards an integrated view of Wnt signaling in development. *Development* **136**, 3205-3214. doi:10.1242/dev.033910
- van den Heuvel, M., Harryman-Samos, C., Klingensmith, J., Perrimon, N. and Nusse, R.** (1993). Mutations in the segment polarity genes *wingless* and *porcupine* impair secretion of the *wingless* protein. *EMBO J.* **12**, 5293-5302. doi:10.1002/j.1460-2075.1993.tb06225.x
- Viadar, E. K., Antic, D. and Axelrod, J. D.** (2009). Planar cell polarity signaling: the developing cell's compass. *Cold Spring Harb. Perspect. Biol.* **1**, a002964-a002964. doi:10.1101/cshperspect.a002964
- Viadar, E. K., Bayly, R. D., Sangoram, A. M., Scott, M. P. and Axelrod, J. D.** (2012). Microtubules enable the planar cell polarity of airway cilia. *Curr. Biol.* **22**, 2203-2212. doi:10.1016/j.cub.2012.09.046
- Wang, Y. and Nathans, J.** (2007). Tissue/planar cell polarity in vertebrates: new insights and new questions. *Development* **134**, 647-658. doi:10.1242/dev.02772
- Wang, J., Mark, S., Zhang, X., Qian, D., Yoo, S.-J., Radde-Gallwitz, K., Zhang, Y., Lin, X., Collazo, A., Wynshaw-Boris, A. et al.** (2005). Regulation of polarized

- extension and planar cell polarity in the cochlea by the vertebrate PCP pathway. *Nat. Genet.* **37**, 980-985. doi:10.1038/ng1622
- Wang, J., Hamblet, N. S., Mark, S., Dickinson, M. E., Brinkman, B. C., Segil, N., Fraser, S. E., Chen, P., Wallingford, J. B. and Wynshaw-Boris, A.** (2006a). Dishevelled genes mediate a conserved mammalian PCP pathway to regulate convergent extension during neurulation. *Development* **133**, 1767-1778. doi:10.1242/dev.02347
- Wang, Y., Guo, N. and Nathans, J.** (2006b). The role of Frizzled3 and Frizzled6 in neural tube closure and in the planar polarity of inner-ear sensory hair cells. *J. Neurosci.* **26**, 2147-2156. doi:10.1523/JNEUROSCI.4698-05.2005
- White, J. J., Mazzeu, J. F., Coban-Akdemir, Z., Bayram, Y., Bahrambeigi, V., Hoischen, A., van Bon, B. W. M., Gezdirici, A., Gulec, E. Y., Ramond, F. et al.** (2018). WNT signaling perturbations underlie the genetic heterogeneity of Robinow syndrome. *Am. J. Hum. Genet.* **102**, 27-43. doi:10.1016/j.ajhg.2017.10.002
- Wu, J., Roman, A.-C., Carvajal-Gonzalez, J. M. and Mlodzik, M.** (2013). Wg and Wnt4 provide long-range directional input to planar cell polarity orientation in *Drosophila*. *Nat. Cell Biol.* **15**, 1045-1055. doi:10.1038/ncb2806
- Yamamoto, S., Nishimura, O., Misaki, K., Nishita, M., Minami, Y., Yonemura, S., Tarui, H. and Sasaki, H.** (2008). Cthrc1 selectively activates the planar cell polarity pathway of Wnt signaling by stabilizing the Wnt-receptor complex. *Dev. Cell* **15**, 23-36. doi:10.1016/j.devcel.2008.05.007
- Yin, H., Copley, C. O., Goodrich, L. V. and Deans, M. R.** (2012). Comparison of phenotypes between different vangl2 mutants demonstrates dominant effects of the Looptail mutation during hair cell development. *PLoS ONE* **7**, e31988. doi:10.1371/journal.pone.0031988
- Zakaria, S., Mao, Y., Kuta, A., de Sousa, C. F., Gaufo, G. O., McNeill, H., Hindges, R., Guthrie, S., Irvine, K. D. and Francis-West, P. H.** (2014). Regulation of neuronal migration by Dchs1-Fat4 planar cell polarity. *Curr. Biol.* **24**, 1620-1627. doi:10.1016/j.cub.2014.05.067

Supplementary Materials and Methods:

Permutation tests (R script):

The functions takes 4 arguments: a vector (x) containing all the angular observations; a vector (*subject*) of the same length that specifies from which mouse each observation comes from; another vector (*Group*) of the same length that specifies to which group the mouse belongs; and finally the number (B) of permutations to be run to calculate the p-value. Note: Install the R package 'circular' (<https://www.rdocumentation.org/packages/circular.>) before running tests.

To test changes in mean orientation:

```
angular.meanG.test<-function(x,subject,Group,B)
{
  m<-length(x)
  s<-levels(as.factor(subject))
  ns<-length(levels(as.factor(subject[Group==levels(as.factor(Group))[1]])))
  observed<-abs(mean.circular(x[Group==levels(as.factor(Group))[1]])-
mean.circular(x[Group!=levels(as.factor(Group))[1]]))
  differenza<-NULL
  for(i in 1:B)
  {
    bs<-sample(s,length(s),replace=F)
    sx<-bs[1:ns]
    group1<-x[subject %in% sx]
    group2<-x[subject %in% bs[-c(1:ns)]]
    differenza<-c(differenza,abs(mean.circular(group1)-mean.circular(group2)))
  }
}
```



```
return((sum(differenza>observed)+1)/(B+1))
```

```
}
```

To test changes in variance:

```
angular.IntraVarG.test<-function(x,subject,Group,B)
```

```
{
```

```
  m<-length(x)
```

```
  s<-levels(as.factor(subject))
```

```
  ms<-tapply(x,as.factor(subject),mean.circular)
```

```
  cx<-x
```

```
  for(i in 1:length(s))
```

```
    { cx[subject==s[i]]<-x[subject==s[i]]-ms[i]
```

```
    }
```

```
  ns<-length(levels(as.factor(subject[Group==levels(as.factor(Group))[1]])))
```

```
  observed<-abs(var.circular(cx[Group==levels(as.factor(Group))[1]])-  
var.circular(cx[Group!=levels(as.factor(Group))[1]]))
```

```
  diff<-NULL
```

```
  for(i in 1:B)
```

```
  {
```

```
    bs<-sample(s,length(s),replace=F)
```

```
    sx<-bs[1:ns]
```

```
    group1<-cx[subject %in% sx]
```

```
    group2<-cx[subject %in% bs[-c(1:ns)]]
```

```
    diff<-c(diff,abs(var.circular(group1)-var.circular(group2)))
```

```
  }
```

Figure S1

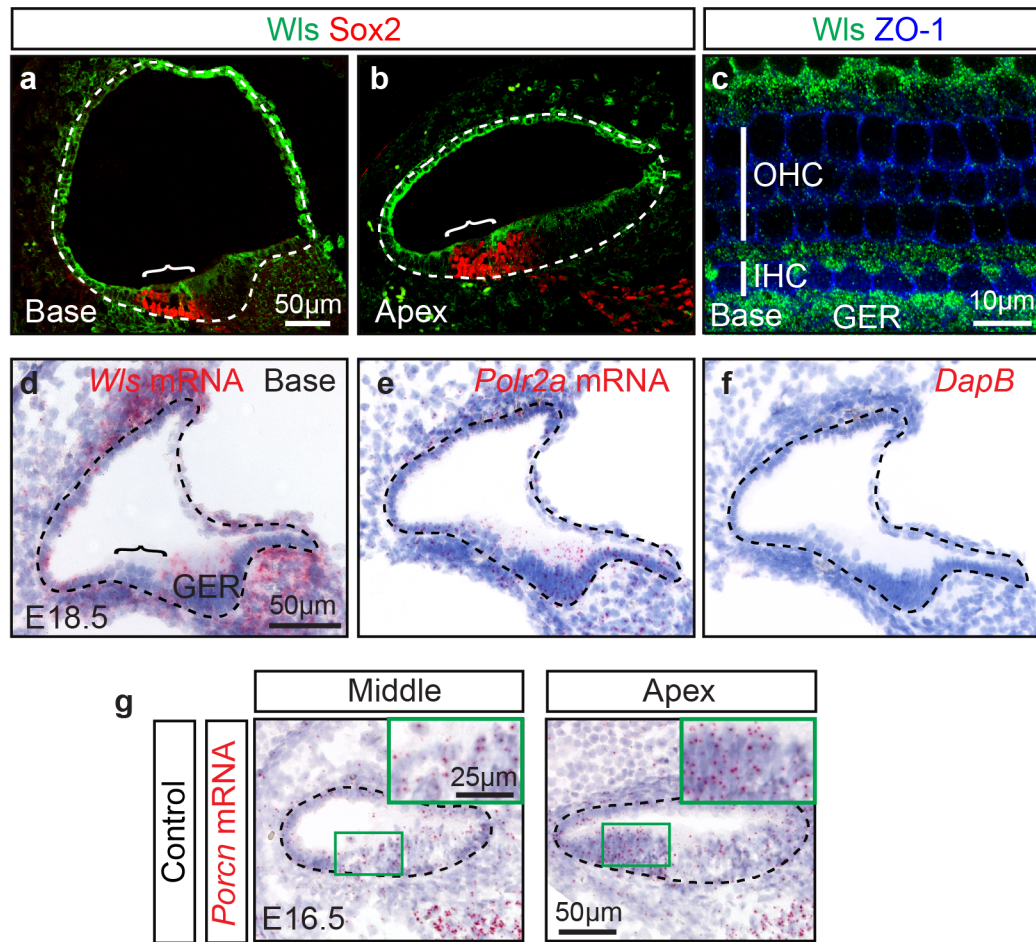


Figure S1. Expression of *Wntless (Wls)* and *Porcupine (Porcn)* in the embryonic cochlea. (a-b) Sections of E18.5 cochlea showing expression of Wls protein in the basal and apical turns. Sox2 marks hair cells and supporting cells in the organ of Corti. c) Whole mount preparation of E18.5 cochlea immunostained for Wls and the junctional marker ZO-1. At this age, Wls expression was detected primarily in supporting cells in the organ of Corti. d) *Wls* mRNA expression within and outside the E18.5 cochlear duct. (e-f) Positive (*Polr2a*) and negative (*DapB*) control *in situ* hybridization experiments on E18.5 cochlea. (g) *Porcn* mRNA was also detected inside the E16.5 cochlear duct. Hematoxylin staining was used as a counterstain in (d-g). Dashed lines and brackets highlight the cochlear duct and organ of Corti, respectively. OHC=outer hair cells, IHC=inner hair cells, GER= greater epithelial ridge. Each experiment was repeated at least three times on wild type cochleae.

Figure S2

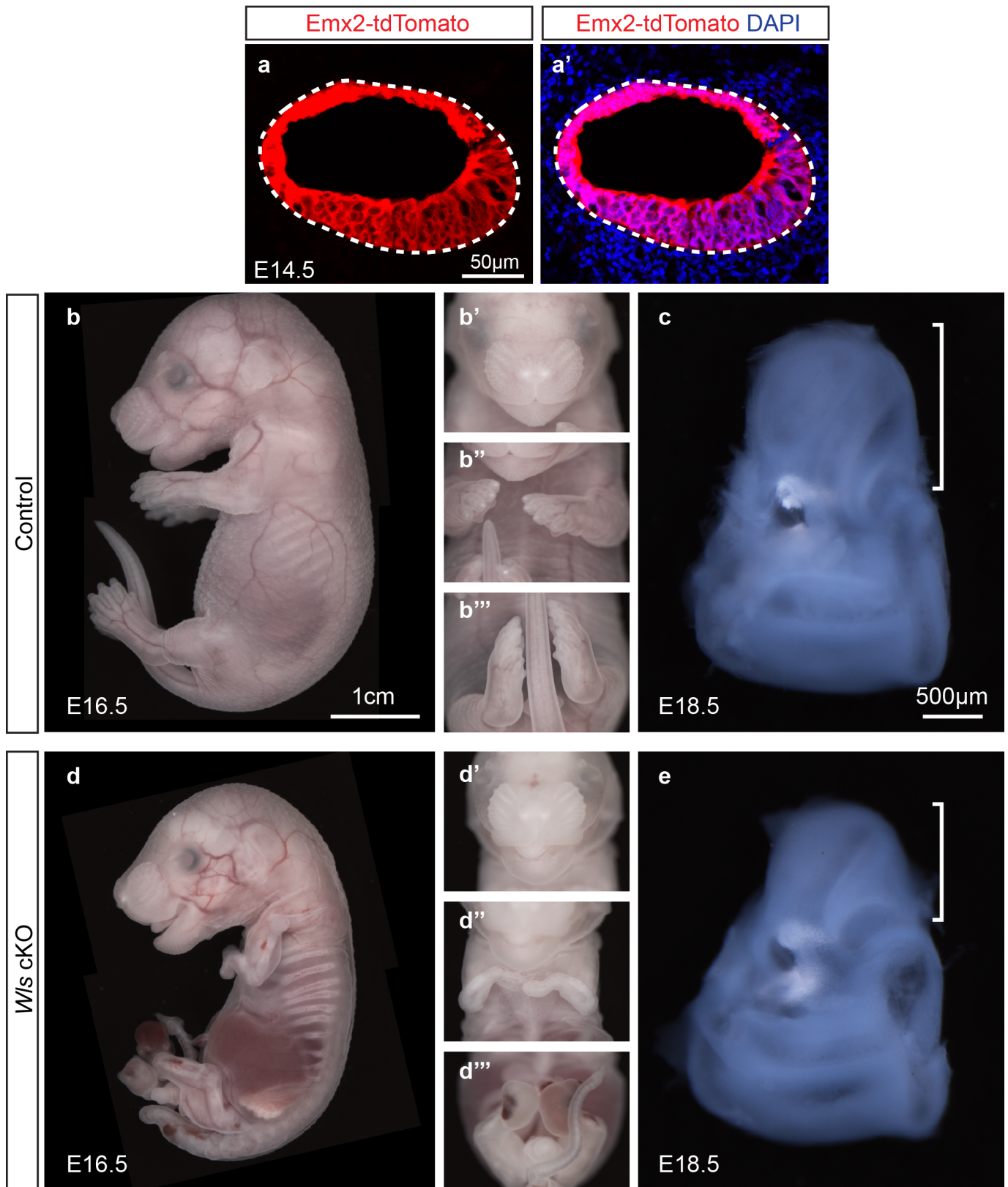


Figure S2. Morphological abnormalities in *Wls* cKO embryos. (a) E14.5 cochlea from *Emx2^{Cre/+}; Rosa26^{tdTomato/+}* mice. Robust tdTomato expression was detected inside the cochlear duct (marked by dashed lines). DAPI (blue) was used to label nuclei. (b) E16.5 control embryos (*Emx2^{Cre/+}; Wls^{+/fl}*). Ventral view of the head (b'), upper limbs (b'') and lower limbs (b'''). (c) Otic capsule from E18.5 control embryos. Bracket marks the cochlea. (d) E16.5 *Wls* cKO embryos (*Emx2^{Cre/+}; Wls^{fl/fl}*) showing craniofacial defects (d'), and underdeveloped upper (d'') and lower (d''') limbs. (e) Otic capsule of E18.5 *Wls* cKO displaying a short cochlea. Three control and *Wls* cKO animals were analyzed.

Figure S3

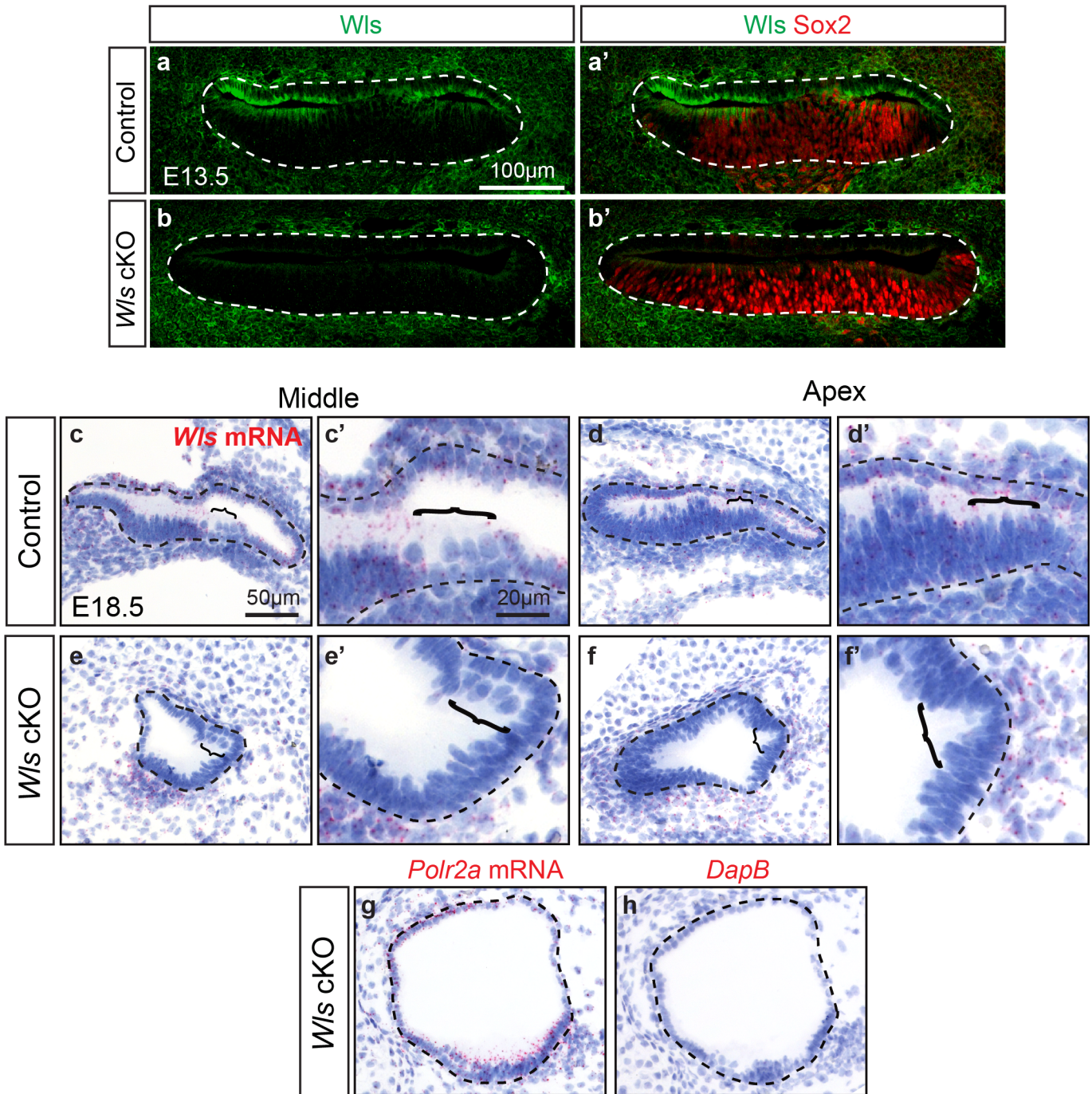


Figure S3. Ablation of *Wls* from the embryonic cochlear duct. (a-b) Cochlear sections from E13.5 control cochlea ($Emx2^{Cre/+}; Wls^{+/fl}$), displaying *Wls* immunofluorescence in the cochlear duct. In contrast, *Wls* expression was absent in the cochlear duct of *Wls* cKO ($Emx2^{Cre/+}; Wls^{fl/fl}$) mice. Of note, *Wls* expression was detected outside the duct in both control and *Wls* cKO cochleae. The prosensory marker *Sox2* was present in both control and *Wls* cKO cochleae. (c-f) *Wls in situ* hybridization in sections from the middle and apical turns of E18.5 control and *Wls* cKO cochleae. *Wls* mRNA was detected in the control cochlea but absent in *Wls* cKO cochlear duct. Higher magnification images of the organ of Corti (marked by brackets) are shown in (c', d', e' and f'). See Supplementary Figure 5 for location of the organ of Corti in *Wls* cKO cochlea. (g-h) Positive (*Polr2a*) and negative (*DapB*) control probes are shown in *Wls* cKO cochlear tissues, respectively. Dashed lines demark the cochlear duct. Hematoxylin (blue) was used to label nuclei. Each experiment was repeated at least three times.

Figure S4

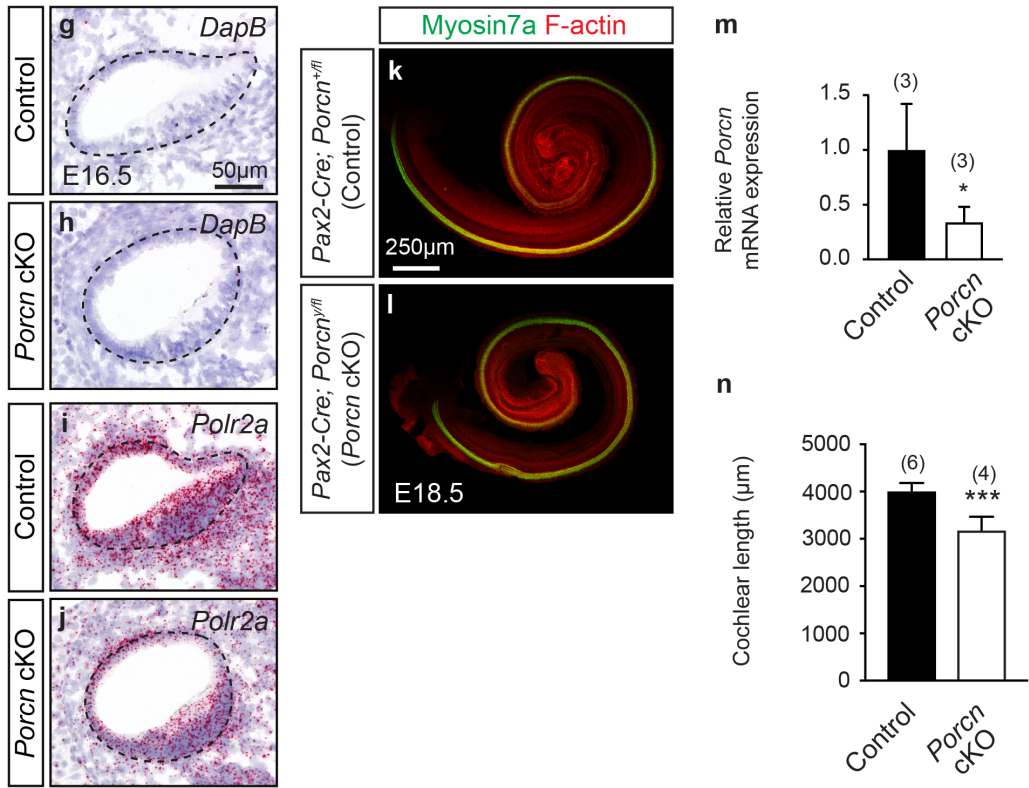
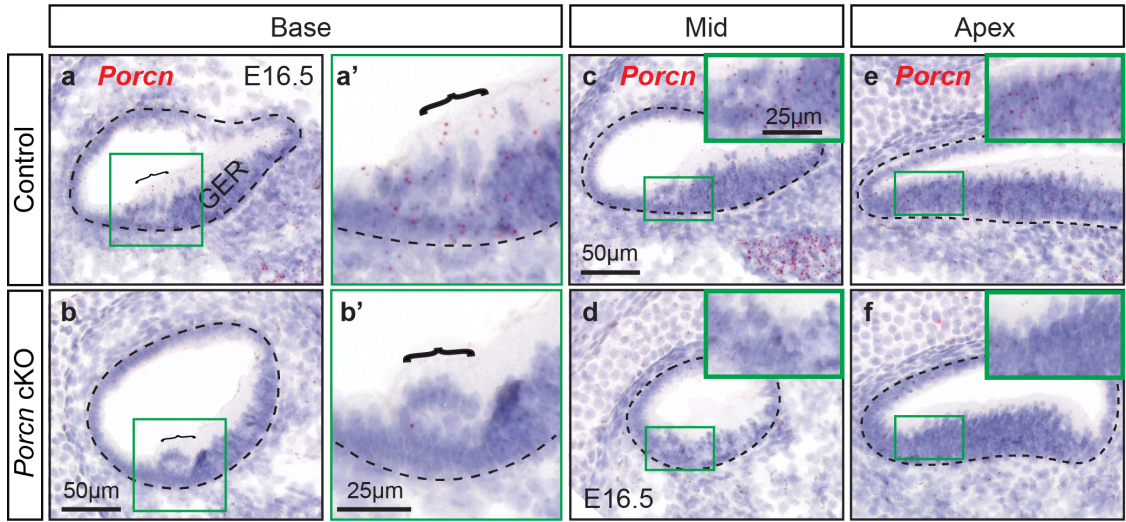


Figure S4. Genetic ablation of *Porcn* from the embryonic cochlear duct. (a-f) *In situ* hybridization (ISH) showing *Porcn* mRNA expression throughout the basal (a), middle (c) and apical (e) turns in sections of control (*Pax2^{Cre/+}; Porcn^{+fl}*) cochleae. (a') high magnification image of the organ of Corti (brackets) showing *Porcn* mRNA expression. In contrast, *Porcn* mRNA signal was drastically reduced in each turn in *Porcn* cKO cochleae (*Pax2-Cre; Porcn^{fl/y}*) (b, d and f), including the organ of Corti (b'). Dashed lines highlight the cochlear duct. (g-j) ISH using negative (*DapB*) and positive (*Polr2a*) control probes in control (g and i) and *Porcn* cKO tissues (h and j). Hematoxylin was used as a counterstain in the ISH experiments. *In situ* probes that hybridize within the floxed exons 3-7 of *Porcn* were used. (k-l) Whole mounts of control (k) and *Porcn* cKO (l) cochleae labeled for Myosin7a (hair cells) and F-actin. *Porcn* cKO cochlea displayed hair cells but appeared dysmorphic and short. Detection for *Porcn* mRNA, Myosin7a and F-actin in control and *Porcn* cKO cochleae was repeated at least three times. (m) qPCR of *Porcn* mRNA showing a significant decrease in *Porcn* cKO cochleae relative to controls (n) *Porcn* cKO cochleae were significantly shorter than controls. Two-tailed t-test, * P < 0.05, ***P < 0.001. Data shown as mean±S.D. GER=Greater epithelial ridge.

Figure S5

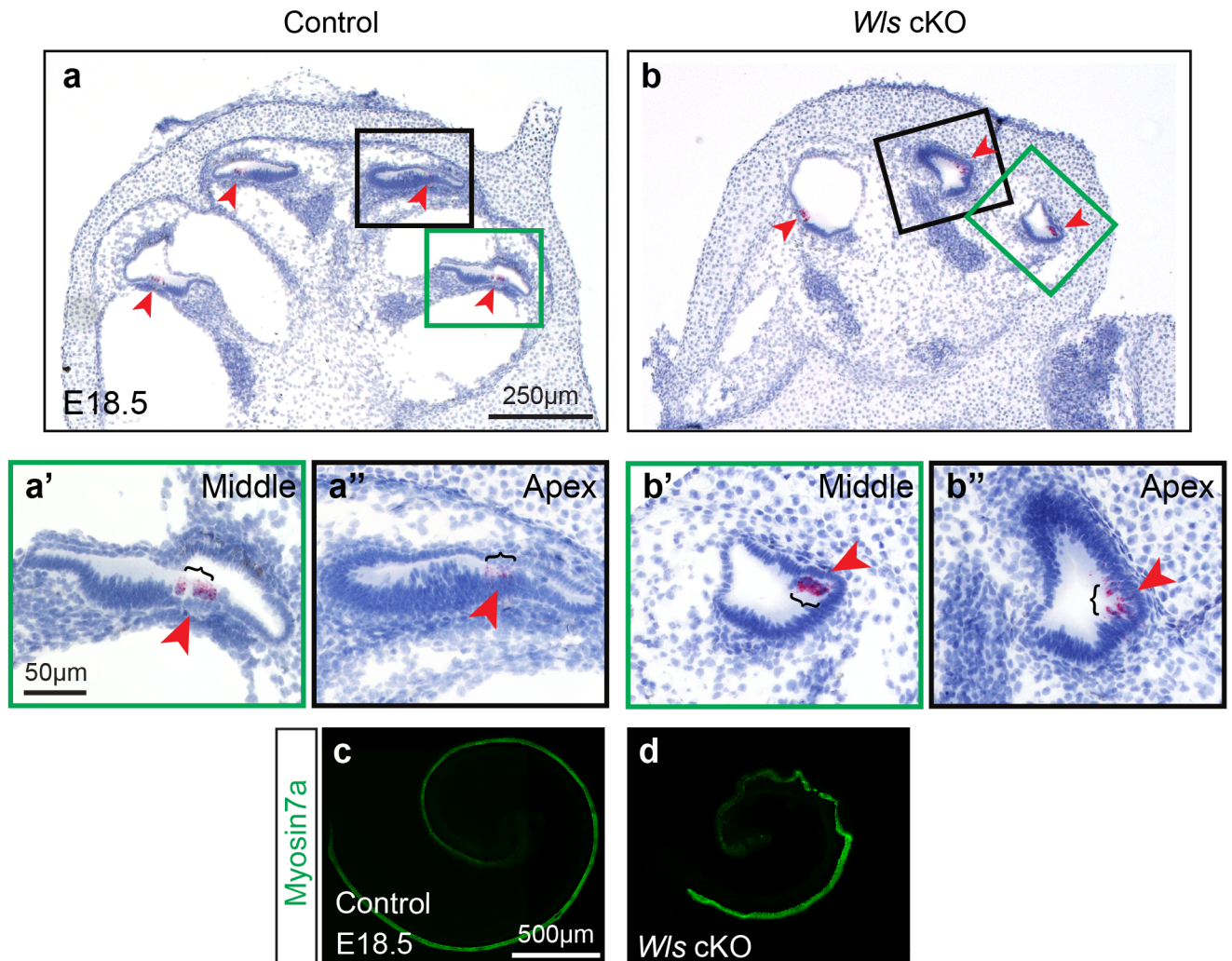


Figure S5. *Wls* is dispensable for hair cell specification. (a-b) *In situ* hybridization for *Atoh1* mRNA in sections of E18.5 control and *Wls* cKO cochleae. *Atoh1*-positive hair cells (red arrows) were found in each turn of E18.5 control cochlea. Middle (a') and apical (a'') turns shown. Though severely dysmorphic, *Wls* cKO cochleae similarly displayed *Atoh1*-positive hair cells. Middle (b') and apical (b'') turns shown. Brackets mark the organ of Corti. Sections were counterstained with hematoxylin (blue). (c-d) Immunostaining showing Myosin7a expression along the length of both control and *Wls* cKO cochleae (E18.5). *Wls* cKO cochleae appeared dysmorphic and short relative to controls. Each experiment was repeated at least three times.

Figure S6

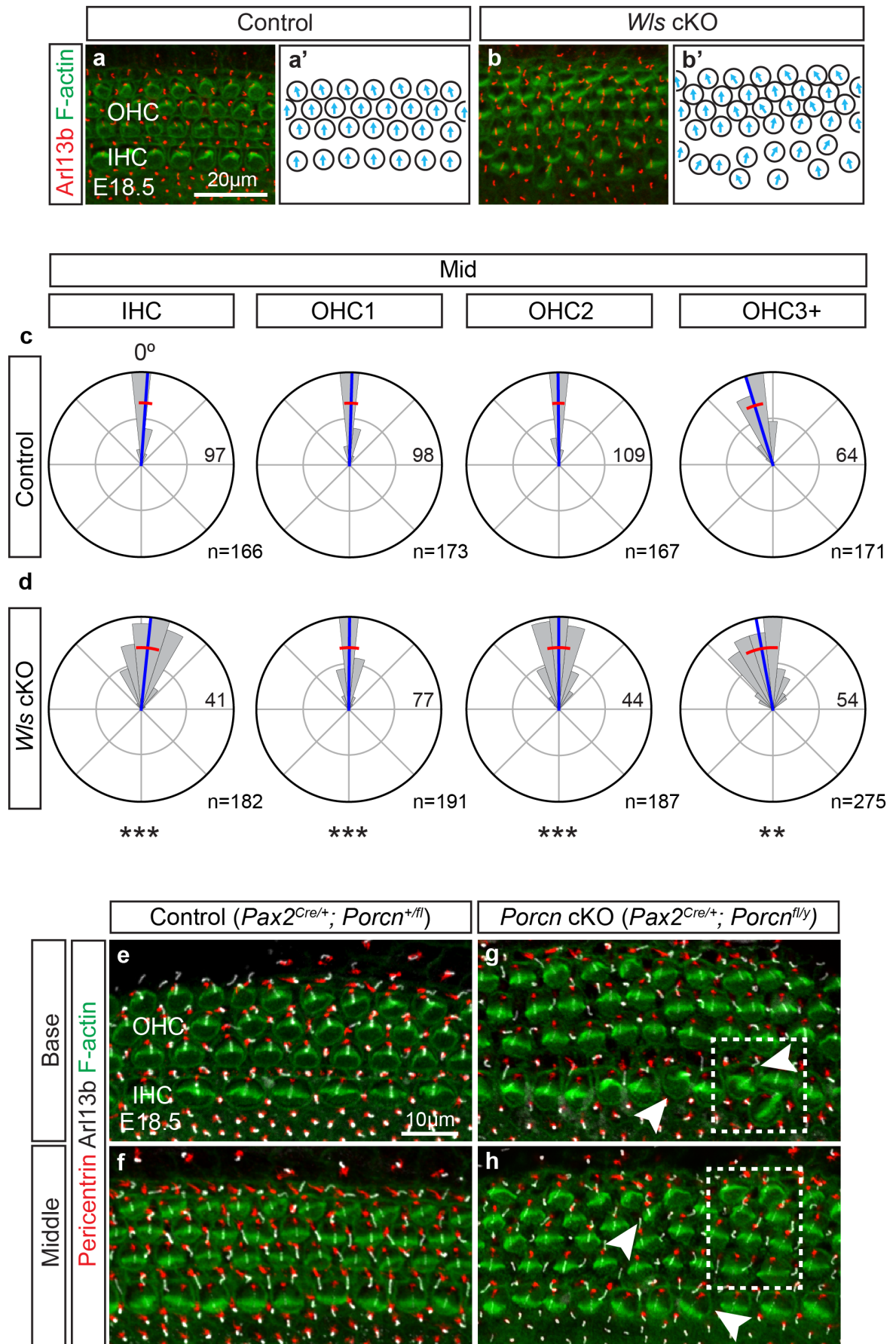


Figure S6. Bundle orientation defects in *Wls* and *Porcn* cKO cochleae. (a-b) E18.5 whole mount cochleae labeled for Arl13b (kinocilium) and F-actin (stereocilia bundles) (middle turn shown). Control cochleae displayed three rows of OHCs and one row of IHCs and stereocilia bundles arranged along the mediolateral axis of the cochlea. In contrast, *Wls* cKO cochleae exhibited supernumerary rows of OHCs and IHCs displaying stereocilia bundles deviated from the mediolateral axis. Panels (a') and (b') show the orientation of individual hair cells in control and *Wls* cKO cochleae, respectively. (c-d) Rose plots depicting the distribution and measurements of stereocilia bundle orientation in control and *Wls* cKO tissues. In comparison to each row of OHCs and IHCs in control cochleae, the variability in the stereocilia bundle orientation of HCs from the *Wls* cKO cochlea was significantly increased. The OHC3+ group included cells from the OHC3 row and OHCs more laterally located. Individual HCs were grouped and plotted into bins 15 degrees wide. The length of each petal represents the number of HCs therein, with the number of the longest petal (also the radius of the outer circle) stated. Radius of inner circle is half of the outer circle. Zero degrees designate the mediolateral axis. Circular mean and circular standard deviation shown in blue and red lines, respectively. (e-h) E18.5 control (*Pax2*^{Cre/+}; *Porcn*^{+/fl}) and *Porcn* cKO (*Pax2*^{Cre/+}; *Porcn*^{fl/y}) cochleae labeled for the basal body (Pericentrin), kinocilium (Arl13b), and F-actin (phalloidin). Basal body/kinocilium were localized to the lateral pole of hair cells in control cochleae and stereocilia bundles were aligned with the mediolateral axis. Basal (e) and middle (f) turns shown. (g-h) On the other hand, *Porcn* cKO cochlea displayed supernumerary IHCs and OHCs (dashed lines), and HCs with defective stereocilia bundle orientation and basal body/kinocilium positioning. Arrowheads mark misoriented HCs. Basal (g) and middle turns (h) shown. n=number of hair cells analyzed from 3 control and *Wls* cKO cochleae. Permutation test of equality of variances used. **p<0.01, ***p<0.001.

Figure S7

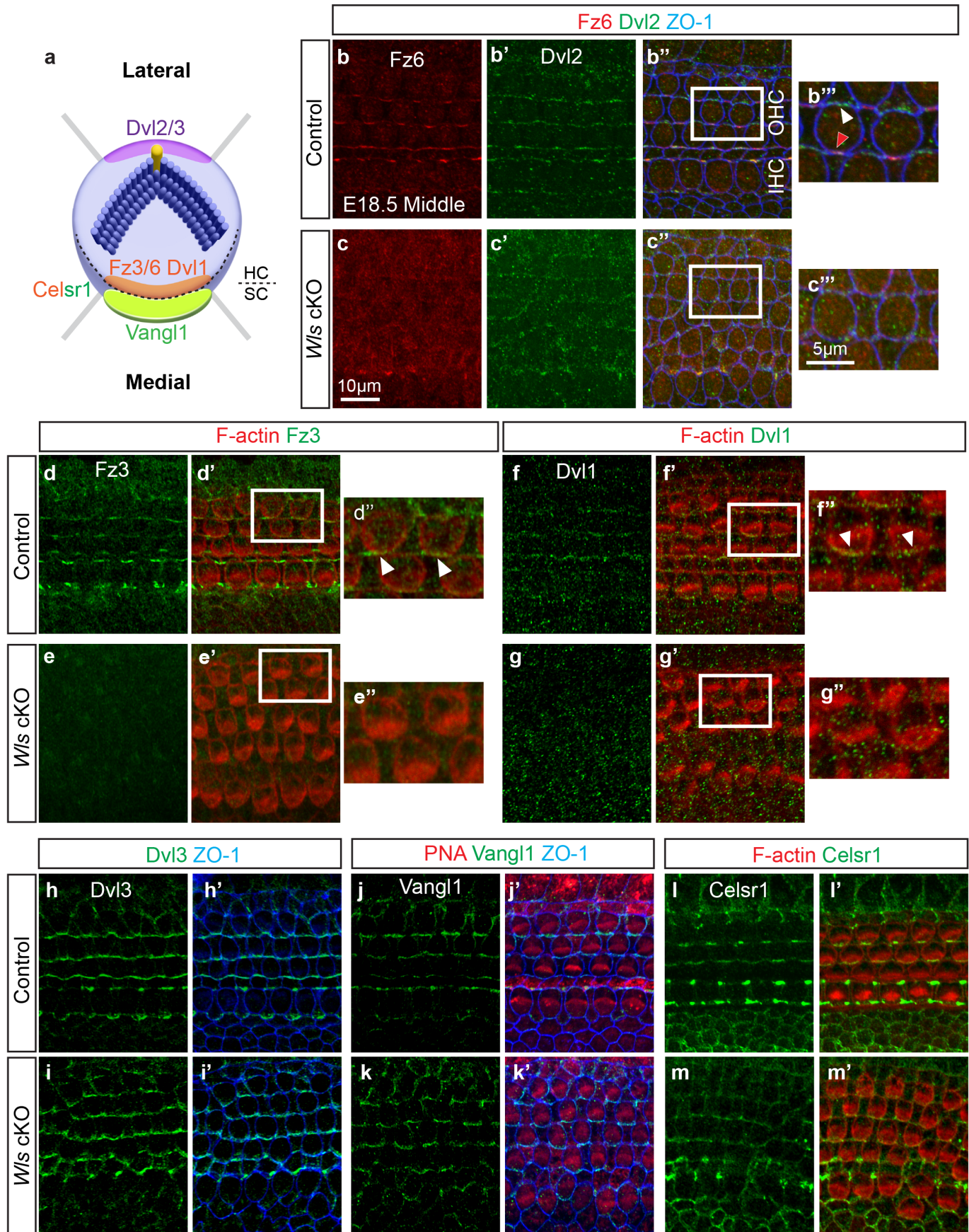


Figure S7. Aberrant localization of planar cell polarity core components in *Wls* cKO cochlea. (a) Cartoon depicting the asymmetric localization of core PCP proteins along the mediolateral axis of hair cells. (b) Representative images acquired from the middle turn of E18.5 control cochlea (*Emx2^{Cre/+}; Wls^{+/fl}*). Fz6 (red arrowhead) and Dvl2 (white arrowhead) were localized to the medial and lateral poles of hair cells (HCs), respectively. Co-staining with the cell junction protein ZO-1 (blue) is shown in panel (b''). (c) No asymmetric localization of Fz6 and Dvl2 was observed in HCs in *Wls* cKO cochlea (*Emx2^{Cre/+}; Wls^{fl/fl}*). Higher magnification of (b'') and (c'') are shown in (b''') and (c'''), respectively. (d) Control cochleae showed Fz3 (green, arrowheads) localized to the medial poles of F-actin-positive HCs. (e) In contrast, no asymmetric localization of Fz3 was observed in *Wls* cKO cochlea. Insets (white boxes) in control (d') and *Wls* cKO cochleae (e') are shown in (d'') and (e''), respectively. (f-g) In control cochlea, Dvl1 signal was mainly detected at the medial junctions of HCs with adjacent supporting cells (arrowheads). No asymmetric localization of Dvl1 was observed in HCs in *Wls* cKO. Higher magnification of insets in (f) and (g') are shown in (f'') and (g''), respectively. (h) Co-staining for Dvl3 with ZO-1 indicated localization of Dvl3 to the lateral side of HCs in both control and *Wls* cKO cochleae. (j-m) Comparable expression patterns of *Vangl1* and *Celsr1* were observed in both control and *Wls* cKO cochleae. Peanut agglutinin (PNA) and phalloidin marked F-actin-enriched HC bundles.

Figure S8

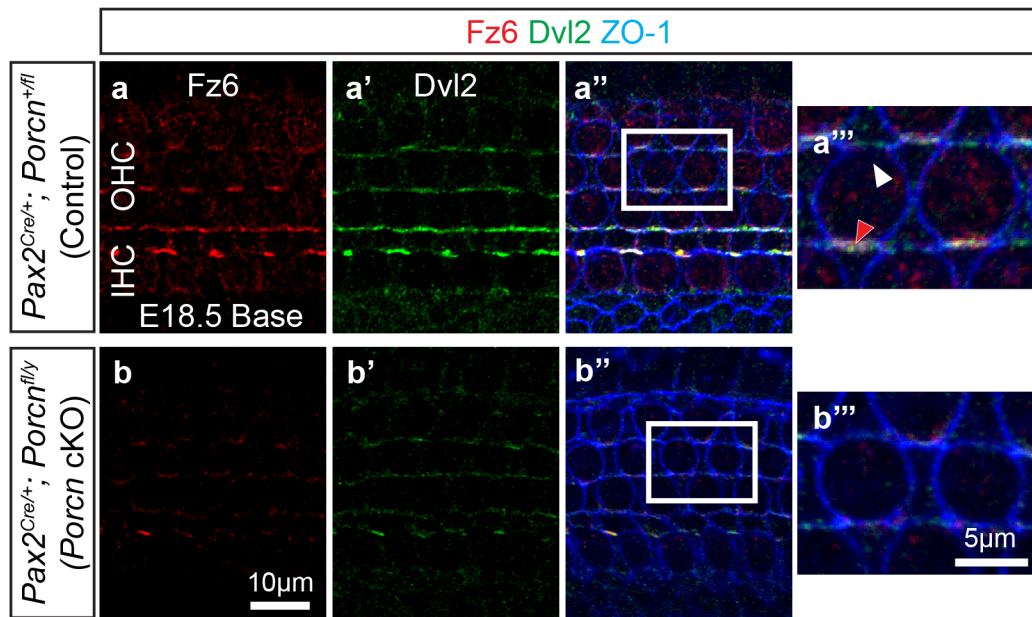


Figure S8. Abnormal localization of planar cell polarity core proteins in *Porcn* cKO cochlea. (a-b) Whole mount cochleae from E18.5 control ($Pax2^{Cre/+}; Porcn^{+/fl}$) and *Porcn* cKO ($Pax2^{Cre/+}; Porcn^{fl/y}$) mice immunostained for Fz6 (red), Dvl2 (green) and ZO-1 (blue). Control cochleae showed expression of Fz6 (red arrowhead) and Dvl2 (white arrowhead) restricted to the medial and lateral poles of HCs, respectively. In contrast, localized expression of Fz6 (b) and Dvl2 (b') was sharply decreased in *Porcn* cKO cochlea. High magnification images of insets (white boxes) in panels (a'') and (b'') are shown in (a''') and (b'''), respectively.

Figure S9

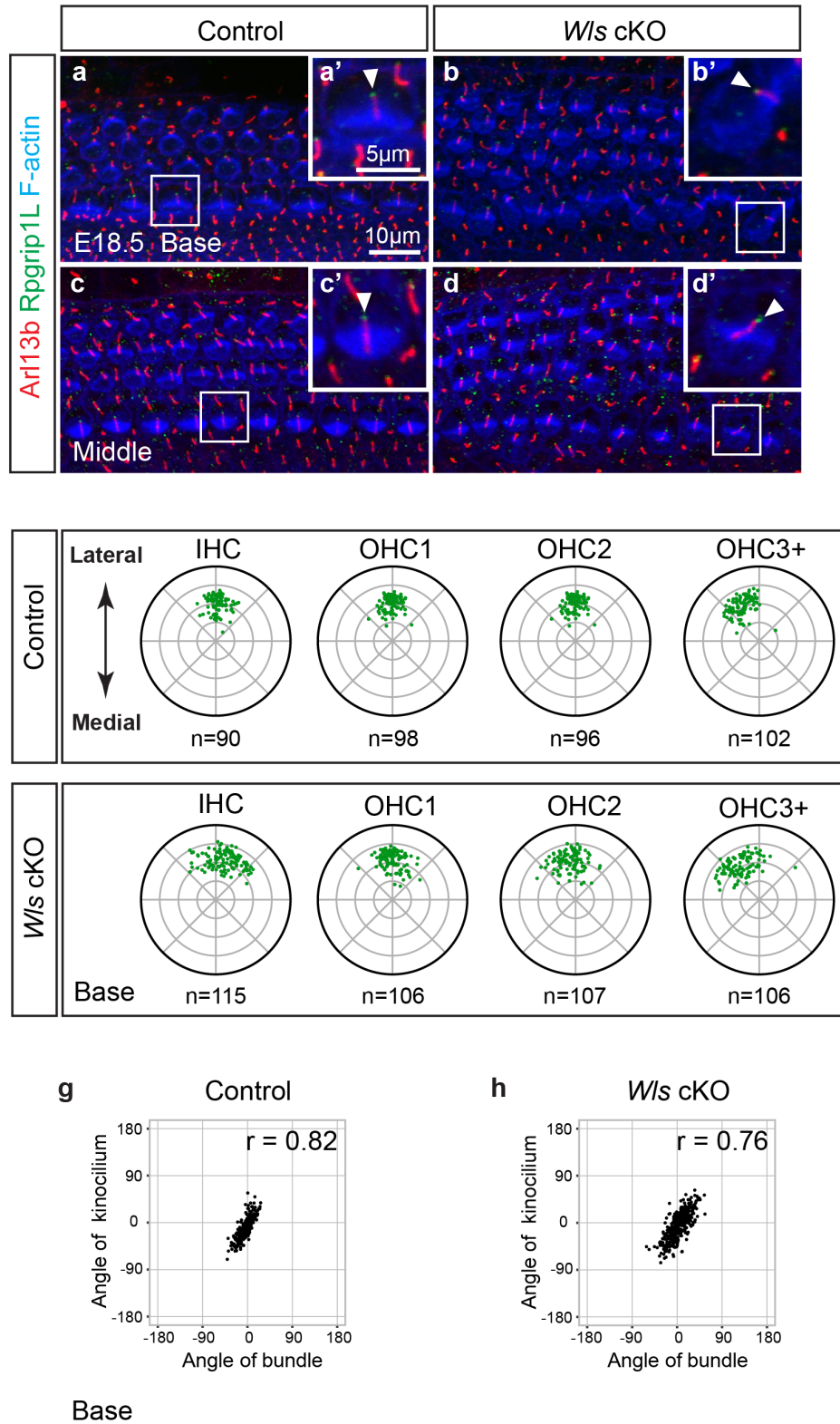


Figure S9. Aberrant kinocilium positioning in *Wls* cKO cochlea. (a-d) Cochlear whole mounts stained for Arl13b, Rpgrip1L and F-actin to label the kinocilium, transitional zone and stereocilia bundles, respectively. Basal and middle turns shown. In control cochlea (*Emx2^{Cre/+}; Wls^{+/fl}*), both Arl13b and Rpgrip1L (arrowheads) were located at the lateral pole of OHCs and IHCs and stereociliary bundles were uniformly oriented along the mediolateral axis. In contrast, *Wls* cKO (*Emx2^{Cre/+}; Wls^{fl/fl}*) tissues showed malpositioned kinocilium (arrowheads) and misoriented stereocilia bundles (b and d). Higher magnifications of insets (white boxes) in (a-d) are shown in (a'-d'). (e) Scatter plots of kinocilium position (based on Rpgrip1L expression) in hair cells from basal turn of E18.5 control cochlea. Kinocilium positions were tightly clustered at the lateral pole of each row of hair cells. (f) In *Wls* cKO cochlea, the kinocilium position was more scattered in comparison to controls. The OHC3+ group included cells from the OHC3 row and OHCs more laterally located. In the scatter plots, concentric circles indicate relative distance from the center of the apical surface of HCs. n=HC number analyzed from 3 control and *Wls* cKO cochleae. (g-h) The angular position of kinocilium and the angle of stereocilia bundle orientation were highly correlated in both control (Pearson_{circular} correlation test, $r=0.82$, $n=386$, $p<0.001$) and *Wls* cKO cochleae (Pearson_{circular} correlation test, $r=0.76$, $n=434$, $p<0.001$).

Figure S10

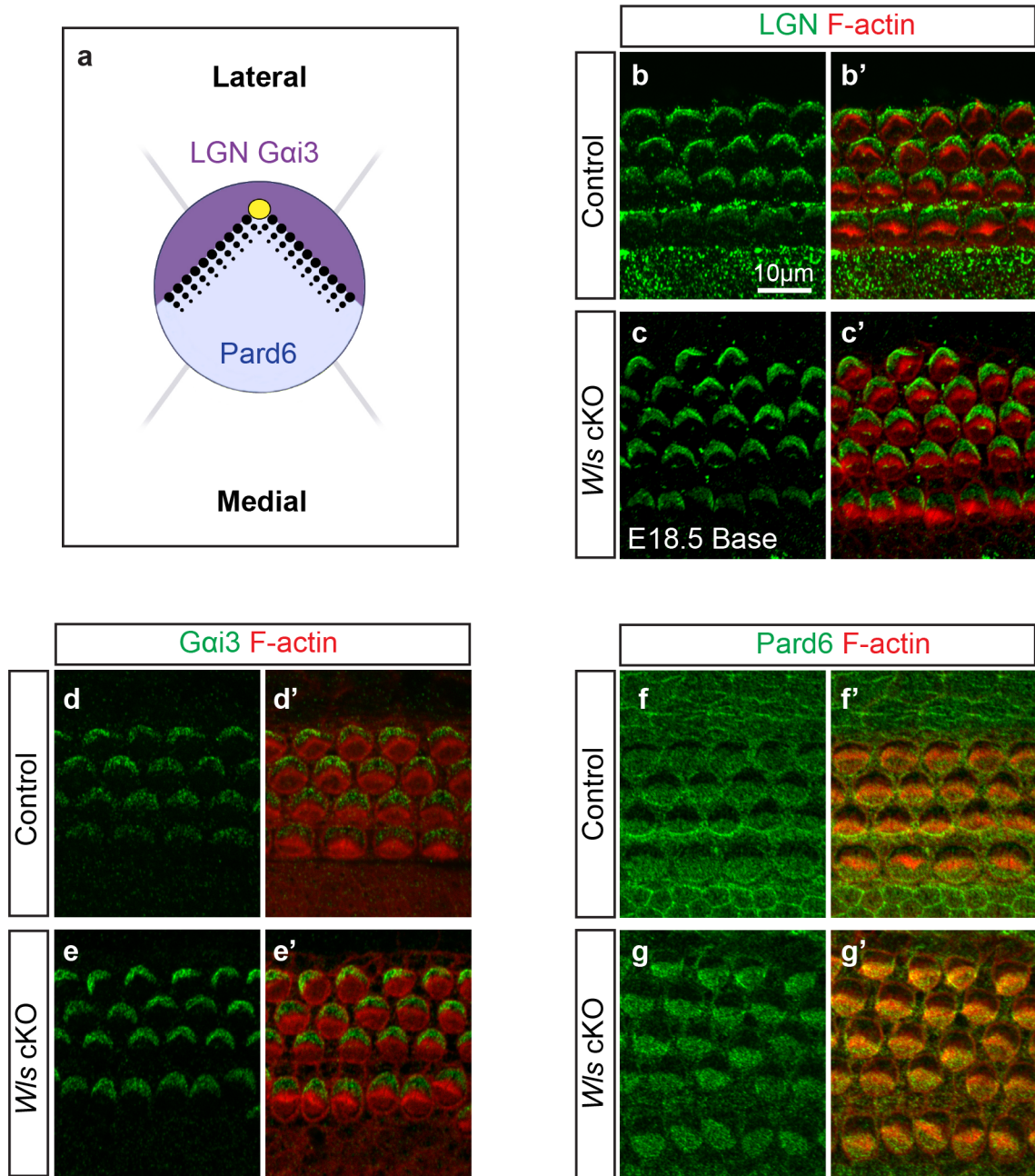


Figure S10. *Wis* is dispensable for the asymmetric distribution of intrinsic polarity proteins. (a) Cartoon depicting the asymmetric distribution of intrinsic polarity proteins in the apical surface of HCs. LGN and Gai3 are both located on the lateral side and Pard6 on the medial side of hair cells. (b-c) In control ($Emx2^{Cre/+}; Wis^{+/fl}$) and *Wis* cKO ($Emx2^{Cre/+}; Wis^{fl/fl}$) cochleae (basal turn, E18.5), LGN (green) was present in the lateral side of hair cells. Bundles were stained for F-actin (red). (d-e) Gai3 was found localized to the lateral side of HCs in both control and *Wis* cKO tissues. (f-g) Pard6 was localized to the medial side of HCs in both control and *Wis* cKO cochleae.

Figure S11

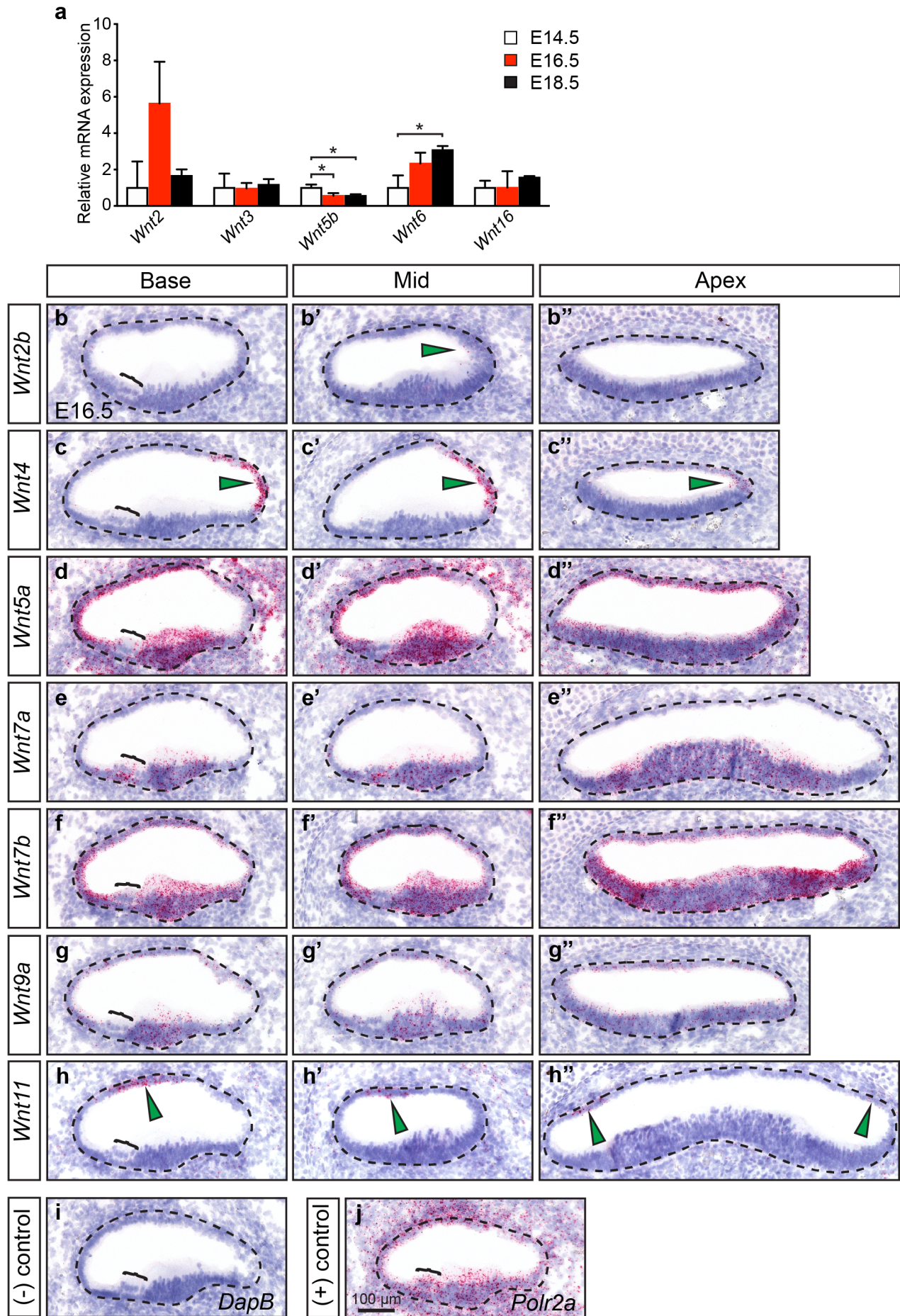


Figure S11. Expression of Wnt ligands in E16.5 cochlear duct. (a) qPCR of Wnt ligands during cochlear development. n=3 for each age group. (b-b'') *In situ* hybridization detecting a low level of *Wnt2b* mRNA in the medial aspect of the cochlear duct (marked by dashed line) in the middle turn. (c-c'') A distinct *Wnt4* expression domain was observed in the medial cochlear roof, most notably in the basal and middle turns. (d-d'') *Wnt5a* was robustly expressed throughout the cochlear duct. (e-e'') *Wnt7a* mRNA was mostly detected in the cochlear floor, whereas *Wnt7b* mRNA (f-f'') was expressed throughout the cochlear duct. (g-g'') A low level of *Wnt9a* expression was noted throughout the cochlear duct. (h-h'') *Wnt11* expression was found in the roof of the cochlea, most notably in the basal turn. (i-j) *DapB* and *Polr2a* were used as negative and positive control probes, respectively. In addition, hematoxylin (blue) was used as counterstain. Arrowheads highlight mRNA signals, whereas brackets indicate the organ of Corti. Each experiment was repeated at least three times. Two-tailed Student's t-test. *P<0.05. Data shown as mean±S.D.

Figure S12

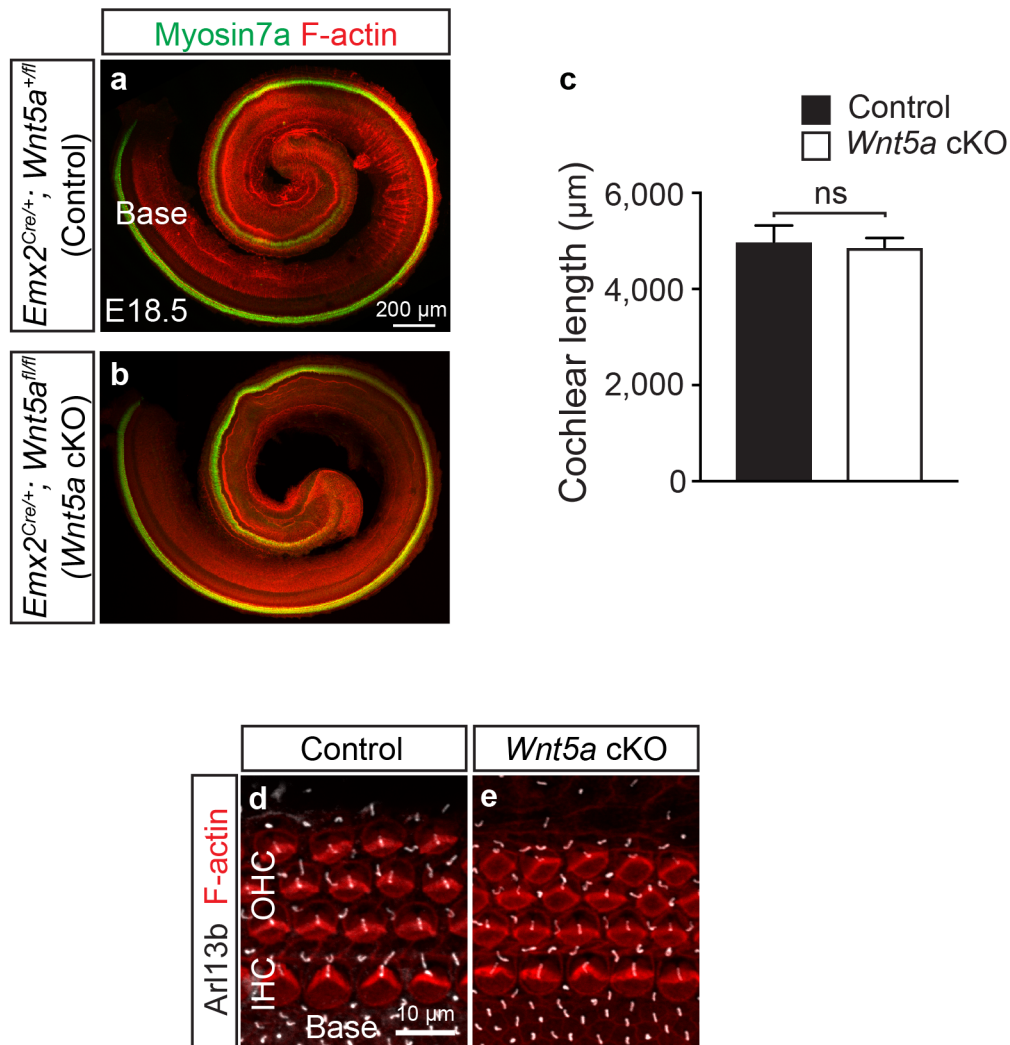


Figure S12. Genetic ablation of *Wnt5a* from the cochlear duct. (a-b) E18.5 whole cochlear mounts stained for Myosin7a (green, hair cells) and F-actin (red). In comparison to controls ($Emx2^{Cre/+}; Wnt5a^{+/fl}$), $Wnt5a$ cKO ($Emx2^{Cre/+}; Wnt5a^{fl/fl}$) cochleae showed no gross disorganization of HCs or decrease in length. (c) No significant differences in length were observed between $Wnt5a$ cKO and control cochleae. $n=3$ per each genotype. (d-e) Both control and $Wnt5a$ cKO tissues displayed three rows of OHCs and one row of IHCs. No misorientation of stereocilia bundles or mislocalization of Arl13b-labeled kinocilium was noted in the $Wnt5a$ cKO cochleae. Student's t-test used, ns= not significant. Data shown as mean \pm S.D.

Figure S13. *Vangl2* genetically interacts with *Wls* to regulate PCP. (a) Schematic illustrating the asymmetric localization of *Vangl2* (green) at the lateral side of supporting cells. (b-c) *Vangl2* was asymmetrically localized in both control ($Emx2^{Cre/+}; Wls^{+/fl}$) and *Wls* cKO ($Emx2^{Cre/+}; Wls^{fl/fl}$) cochleae. ZO-1 and PNA mark tight junctions and stereocilia bundles, respectively. All the images correspond to the middle turn of the cochlea. High magnification images showing *Vangl2* expression in control (b' and b'') and *Wls* cKO tissues (c' and c''). Dashed circles demark cell boundaries and white arrowheads highlight *Vangl2* immunolocalization. (d-e) E18.5 cochleae were double stained for Pericentrin (red) and F-actin (green) to label basal bodies and stereocilia bundles in HCs, respectively. (d) In control ($Emx2^{Cre/+}; Wls^{+/fl}; Vangl2^{Lp/+}$), bundle orientation and basal body positioning appeared normal for IHCs and OHCs. No extranumerary HCs were observed in control cochlea (d and d'). (e) In contrast, *Wls* cKO; $Vangl2^{Lp/+}$ ($Emx2^{Cre/+}; Wls^{fl/fl}; Vangl2^{Lp/+}$) cochlea displayed many misoriented stereocilia bundles and malpositioned basal bodies (arrows). In addition, extranumerary OHCs were observed in these tissues. In (d) and (e), arrows indicate stereocilia bundle orientations. (d'-e') illustrate the orientation of stereocilia bundles from individual HCs in panels (d-e), respectively. (f-g) Rose and scatter plots depicting the distribution of stereocilia bundle orientation and basal body positioning, respectively. (f) In control, HCs displayed stereocilia bundles aligned in the mediolateral axis and tightly clustered basal bodies at the lateral pole. The third row of OHCs were consistently rotated minus 30 degrees along the mediolateral axis of the cochlea (towards the apex) and with their basal bodies clustered at that angle. In contrast, in *Wls* cKO; $Vangl2^{Lp/+}$ cochleae, HCs showed significantly more variable bundle orientation, particularly among the outermost row of OHCs (Permutation test of equality of variances, $p < 0.001$).

Moreover, basal body positioning in *Wls cKO; Vangl2^{Lp/+}* cochleae was more scattered than in control, particularly in the most lateral outer hair cells. The OHC3+ group included cells from the OHC3 row plus more laterally located OHCs. In the scatter plots, concentric circles indicate relative distance from the center of the apical surface of HCs. n=number of hair cells analyzed from 3 control and *Wls cKO; Vangl2^{Lp/+}* cochleae. Zero degrees designate the mediolateral axis. Permutation test of equality of variances used. ***p<0.001. Circular mean and circular standard deviation shown in blue and red lines, respectively.

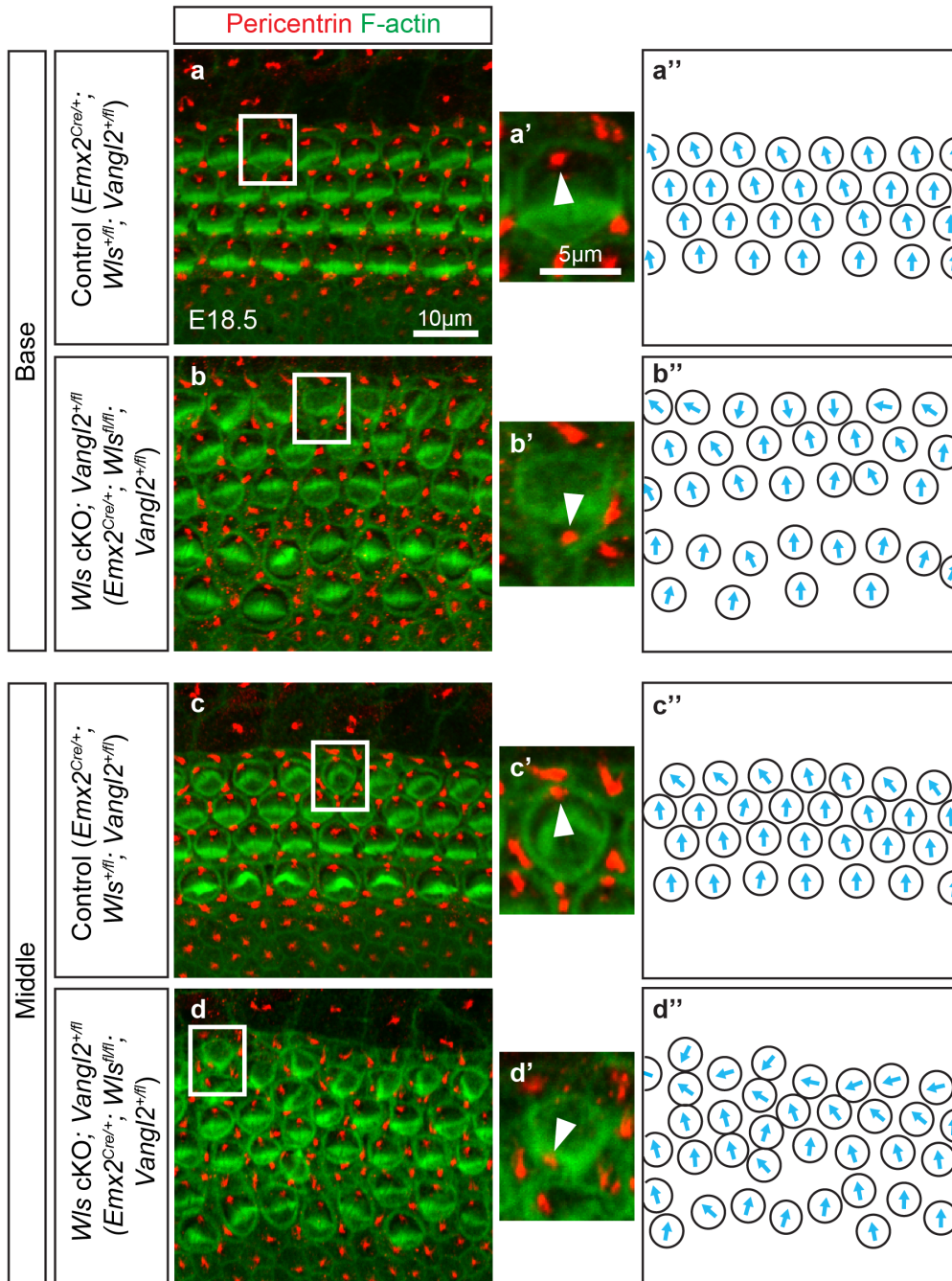


Figure S14. *Vangl2* and *Wls* coordinate to regulate planar polarization. (a-d) Pericentrin (red) and F-actin (green) marked the basal body and stereocilia bundles, respectively, in cochleae from E18.5 control (*Emx2*^{Cre/+}; *Wls*^{+/fl}; *Vangl2*^{+/fl}) and *Wls* cKO; *Vangl2*^{+/fl} (*Emx2*^{Cre/+}; *Wls*^{fl/fl}; *Vangl2*^{+/fl}) animals. Basal and middle turns shown. (a, c) In the control cochleae, stereocilia bundles were uniformly oriented along the mediolateral axis and basal bodies (arrowheads) were mainly located at the lateral pole of hair cells (HCs). There were also no extranumerary HCs. (b, d) In contrast, HCs in *Wls* cKO; *Vangl2*^{+/fl} cochleae showed misoriented bundles along with basal body positioning defects, which were most severe in the outermost row of OHCs. Some OHCs were rotated almost 180 degrees with respect to the mediolateral axis. In addition, extranumerary IHCs and OHCs were observed in *Wls* cKO; *Vangl2*^{+/fl} cochleae. Insets (white boxes) in control and *Wls* cKO; *Vangl2*^{+/fl} tissues are shown in panels (a', c') and (b', d'), respectively. Arrowheads mark the position of basal bodies. For panels (a-d), the orientation of each hair cell is illustrated in (a''-d''), respectively. Three control and *Wls* cKO; *Vangl2*^{+/fl} cochleae were analyzed.

Table S1. qPCR primer sequences

Gene Name	Forward primer (5' -> 3')	Reverse primer (5' -> 3')	Accession number
<i>Wnt1</i>	CAA ATG GCA ATT CCG AAA CCG	GGA GGT GAT TGC GAA GAT GA	NM_021279.4
<i>Wnt2</i>	GTA GAT GCC AAG GAG AGG AAA G	CAC ACC ATG ACA CTT GCA TTC	NM_023653.5
<i>Wnt2b</i>	CTC ATG AAC TTA CAC AAC AAC CG	CAG AGT ACA GGA GCC ACT CA	NM_009520.3
<i>Wnt3</i>	AGC TGC CAA GAG TGT ATT CG	CAT GGG ACT TCG ATG AAT GGA	NM_009521.2
<i>Wnt3a</i>	ATC TTT GGC CCT GTT CTG G	GAG CGT GTC ACT GCG AA	NM_009522.2
<i>Wnt4</i>	GGC ACT CAT GAA TCT TCA CAA C	GCA CGT CTT TAC CTC GCA	NM_009523.2
<i>Wnt5a</i>	GTG CCA TGT CTT CCA AGT TCT	GTT ATT CAT ACC TAG AGA CCA CCA	NM_009524.3
<i>Wnt5b</i>	CCA ACA CCA GTT TCG ACA GA	AAG GCA GTC TCT CGG CTA	NM_009525.3
<i>Wnt6</i>	GTT CCA GTT CCG TTT CCG A	ATG GAA CAG GCT TGA GTG AC	NM_009526.3
<i>Wnt7a</i>	CAG TTT CAG TTC CGA AAT GGC	GAT AAT CGC ATA GGT GAA GGC A	NM_009527.3
<i>Wnt7b</i>	CCA GCA CCA GTT CCG ATT	CCG TGA TGG CAT AGG TGA A	NM_009528.3
<i>Wnt8a</i>	CAG ACT CTT CGT GGA CAG TT	CCT GAG ATG CCA TGA CAC TT	NM_009290.2
<i>Wnt8b</i>	TGT GCG TTC TTC TAG TCA CTT G	GTA GAC CAG GTA AGC CTT TGG	NM_011720.3
<i>Wnt9a</i>	CAG TAC CAG TTC CGC TTT GAG	GAA GAG ATG GCG TAG AGG AAA	NM_139298.2
<i>Wnt9b</i>	AAG TAC AGC ACC AAG TTC CTC	CAC TTG CAG GTT GTT CTC AG	NM_011719.4
<i>Wnt10a</i>	CTC CTG TTC TTC CTA CTG CTG	ACT GTG TTG GCG TTG AGC	NM_009518.2
<i>Wnt10b</i>	GAT CCT GCA CCT GAA CCG	CCG ACT GAA CAA AGC CAA GA	NM_011718.2
<i>Wnt11</i>	ATG AAG AAT GAG AAG GTG GGA T	GTA CTT GCA GTG ACA TCG CT	NM_001285792.1
<i>Wnt16</i>	GGA ACC CAG GGC AAC TG	CTC TTG CAC AGC TCC TTC TG	NM_053116.4
<i>Wls</i>	TTT CCA AAT CGT TGC CTT TCT G	TGG TTC TTA CGG ACA TCC AC	NM_026582(2)
<i>Porcn</i>	TCC GTC ACC ATC CTC ATC TAC	GAG ACA CCG CCT TCA TGG	NM_016913(4)
<i>Rpl19</i>	GGTCTGGTTGGATCCCAATG	CCCGGGAATGGACAGTCA	NM_009078.2

Table S2. Antibody list.

Protein	Antibody	Source	Dilution
Wls	EUR302	Kerafast	1:10000
Wls	17950-1-AP	Proteintech	1:500
Vangl2	21492-1-AP	Proteintech	1:250
Vangl1	HPA025235	Sigma-Aldrich	1:1000
Fzd6	AF1526	R and D Systems	1:250
Fzd3		gift from Jeremy Nathans	1:500
Celsr1		gift from Elaine Fuchs	1:3000
Dvl1	27384-1-AP	Proteintech	1:250
Dvl2	3224	Cell Signaling Technology	1:250
Dvl2	12037-1-AP	Proteintech	1:250
Dvl3	13444-1-AP	Proteintech	1:1000
Atoh1	21215-1-AP	Proteintech	1:1000
Myo7a	25-6790	Proteus Biosciences	1:1000
Sox2	sc-17320	Santa Cruz	1:200
ZO-1	33-9100	Thermo Scientific	1:1000
Arl13b	75-287	NeuroMab	1:500
Pericentrin	923701	BioLegend	1:1000
Acetylated α -tubulin	T7451	Sigma-Aldrich	1:500
RpGrip1L	55160-1-AP	Proteintech	1:500
Gn α 3	11641-1-AP	Proteintech	1:250
Lgn		gift from Quansheng Du	1:1000
ParD6B	13996-1-AP	Proteintech	1:250